TKK Dissertations 152
Espoo 2009

SURFACE ACOUSTIC WAVE RFID TAGS: IDEAS, DEVELOPMENTS, AND EXPERIMENTS

Doctoral Dissertation

Sanna Härmä

Helsinki University of Technology
Faculty of Information and Natural Sciences
Department of Applied Physics

SURFACE ACOUSTIC WAVE RFID TAGS: IDEAS, DEVELOPMENTS, AND EXPERIMENTS

Doctoral Dissertation

Sanna Härmä

Dissertation for the degree of Doctor of Science in Technology to be presented with due permission of the Faculty of Information and Natural Sciences for public examination and debate in Auditorium AS1 at Helsinki University of Technology (Espoo, Finland) on the 6th of February, 2009, at 12 noon.

Helsinki University of Technology
Faculty of Information and Natural Sciences
Department of Applied Physics

Teknillinen korkeakoulu
Informaatio- ja luonnontieteiden tiedekunta
Teknillisen fysiikan laitos

ABSTRACT OF DOCTORAL DISSERTATION	HELSINKI UNIVERSITY OF TECHNOLOGY P. O. BOX 1000, FI-02015 TKK http://www.tkk.fi

Author	Sanna Katariina Härmä

Name of the dissertation
Surface Acoustic Wave RFID Tags: Ideas, Developments, and Experiments

Manuscript submitted	14.10.2008	Manuscript revised	12.12.2008

Date of the defence	6.2.2009

☐ Monograph	☒ Article dissertation (summary + original articles)

Faculty	Faculty of Information and Natural Sciences
Department	Department of Applied Physics
Field of research	Surface acoustic waves
Opponent(s)	Professor Daniel Hauden
Supervisor	Professor Matti Kaivola
Instructor	Docent Victor P. Plessky

Abstract

Radio-frequency identification (RFID) provides an efficient means of labeling and identifying various items. The principal advantage of RFID over the more traditional barcode labeling is that RFID labels are read using a radio signal. Hence, an unobstructed line-of-sight is not needed between the reader and the label. In addition, RFID labels, or tags, can carry a significantly larger amount of information than barcodes. They also are physically robust whereas printed barcodes can easily be smudged or damaged. Furthermore, it is possible to read many RFID tags simultaneously and the presence of a human operator is generally not needed.

This dissertation focuses on a type of RFID tag that relies on the surface acoustic wave (SAW) technology. SAW RFID tags are passive devices that reflect the interrogation signal in a form that is modified according to the identification information stored on the tag. In reflector-based SAW RFID tags, the encoding is based on the positions of metallic SAW reflectors on the surface of a piezoelectric substrate. In other words, it is based on the time delays of the reflected signals. The dissertation first discusses the extraction of central SAW reflector parameters and then presents novel SAW RFID tag designs. In the first part of the work, the reflectivity of narrow reflector electrodes on $YZ\text{-}LiNbO_3$ substrate is determined. In addition, a new method for extracting the frequency-dependent reflection, transmission, and scattering parameters of short metal reflectors is developed. The second part of the dissertation discusses the design of SAW RFID tags. The main objectives of tag design include the reduction of device size and the enhancement of information capacity. This dissertation presents a Z-path SAW RFID tag that uses two strongly reflecting inclined reflectors to fold the acoustic path. The Z-path SAW tag has a significantly smaller size than previously reported SAW tags. The information capacity of SAW RFID tags is enhanced by combining the conventional time-delay-based encoding with phase encoding. A compact device size and strong resistance to environmental echoes are achieved through the application of ultra-wideband (UWB) radio technology. The feasibility of UWB SAW tags is investigated using simulations and confirmed experimentally. The SAW RFID tags presented in this dissertation are all designed for the $128°\text{-}LiNbO_3$ substrate.

VÄITÖSKIRJAN TIIVISTELMÄ	TEKNILLINEN KORKEAKOULU PL 1000, 02015 TKK http://www.tkk.fi

Tekijä Sanna Katariina Härmä

Väitöskirjan nimi

Akustisiin pinta-aaltoihin perustuvien RFID-tunnisteiden suunnittelu ja kokeellinen analyysi

Käsikirjoituksen päivämäärä 14.10.2008	Korjatun käsikirjoituksen päivämäärä 12.12.2008

Väitöstilaisuuden ajankohta   6.2.2009

☐ Monografia ☒ Yhdistelmäväitöskirja (yhteenveto + erillisartikkelit)

Tiedekunta	Informaatio- ja luonnontieteiden tiedekunta
Laitos	Teknillisen fysiikan laitos
Tutkimusala	akustiset pinta-aallot
Vastaväittäjä(t)	professori Daniel Hauden
Työn valvoja	professori Matti Kaivola
Työn ohjaaja	dosentti Victor P. Plessky

Tiivistelmä

Radiotaajuinen etätunnistus (radio-frequency identification, RFID) on tehokas tapa merkitä ja tunnistaa erilaisia kohteita. Perinteisiin viivakooditunnisteisiin verrattuna RFID-tunnisteiden keskeisin etu liittyy radioaaltojen käyttöön. Suoraa näköyhteyttä tunnisteen ja lukulaitteen välillä ei tarvita. Lisäksi RFID-tunnisteiden informaatiokapasiteetti on merkittävästi suurempi kuin viivakoodien. Ne myös kestävät viivakoodeja paremmin fyysistä kulutusta ja likaisia olosuhteita. RFID-tunnisteet voidaan lukea automaattisesti ilman ihmisen läsnäoloa. Myös useiden tunnisteiden samanaikainen lukeminen on mahdollista.

Tässä väitöskirjassa esitetyn tutkimuksen kohteena ovat RFID-tunnisteet, joiden toiminta perustuu akustisiin pinta-aaltoihin (surface acoustic waves, SAW). SAW RFID -tunnisteet ovat täysin passiivisia laitteita, jotka heijastavat lukulaitteen lähettämän kyselysignaalin takaisin. Paluusignaali on tunnisteelle tallennetun tunnistetiedon mukaisesti muunnetussa muodossa. Väitöskirjassa keskitytään tunnisteisiin, joiden koodaus perustuu pietsosähköisen kiteen pinnalla olevien metallisten SAW-heijastimien sijoitteluun. Työssä käsitellään ensin SAW-heijastimien keskeisten ominaisuuksien määrittämistä ja esitellään sitten uusia SAW RFID -tunnistetyyppejä. Väitöskirjan ensimmäisessä osassa määritetään kapeiden heijastimien heijastavuus YZ-LiNbO$_3$-substraatilla. Lisäksi esitellään uusi menetelmä heijastimien heijastus-, läpäisy-, ja sirontaparametrien määrittämiseksi taajuuden funktiona. Työn toinen osa käsittelee SAW RFID -tunnisteiden suunnittelua. Tunnistesuunnittelun tärkeimpiin tavoitteisiin kuuluvat laitekoon pienentäminen ja informaatiokapasiteetin kasvattaminen. Väitöskirjassa esitellään edeltäjiään merkittävästi pienempi tunniste, jossa akustisen pinta-aallon etenemispolku on taitettu Z-kirjaimen muotoon kahden vinon heijastimen avulla. Toinen esitelty tunniste yhdistää kaksi koodausmenetelmää: heijastimien paikkoihin eli heijastussignaalien aikaviipeisiin perustuvan koodauksen ja heijastussignaalien vaihetietoon perustuvan koodauksen. Tämän yhdistelmän avulla tunnisteen informaatiokapasiteettia voidaan kasvattaa huomattavasti. Kolmas esitelty tunniste soveltaa ultra-laajakaistatekniikkaa (ultra wide band, UWB) ja on erittäin pienikokoinen. Suunnitellun UWB SAW RFID -tunnisteen sisällä tapahtuvan signaalinkäsittelyn ansiosta tunnistuksen alttius ympäristön häiriösignaaleille vähenee. Kaikissa tässä väitöskirjassa esitellyissä SAW RFID -tunnisteissa käytetään 128°-LiNbO$_3$-substraattia.

Asiasanat   akustiset pinta-aallot, RFID

ISBN (painettu) 978-951-22-9742-9	ISSN (painettu) 1795-2239
ISBN (pdf) 978-951-22-9743-6	ISSN (pdf) 1795-4584
Kieli englanti	Sivumäärä 73 s. + liit. 46 s.

Julkaisija   Sanna Härmä

Painetun väitöskirjan jakelu   Teknillinen korkeakoulu, Teknillisen fysiikan laitos

☒ Luettavissa verkossa osoitteessa http://lib.tkk.fi/Diss/2009/isbn9789512297436/

Preface

List of Publications

This dissertation is a review of the author's work in the field of surface acoustic wave technology. It consists of an overview and the following selection of publications in this field:

I S. Härmä, C.-U. Kim, S. M. Balashov, and V. P. Plessky, "Narrow electrodes on YZ-LiNbO$_3$ as an alternative to etched grooves for dispersive delay lines", *IEEE Transactions on Ultrasonics, Ferroelectrics, and Frequency Control* **55**(2), pp. 494-498 (2008).

II S. Härmä and V. P. Plessky, "Extraction of frequency-dependent reflection, transmission, and scattering parameters for short metal reflectors from FEM-BEM simulations", *IEEE Transactions on Ultrasonics, Ferroelectrics, and Frequency Control* **55**(4), pp. 883-889 (2008).

III S. Härmä, V. P. Plessky, C. S. Hartmann, and W. Steichen, "Z-path SAW RFID tag", *IEEE Transactions on Ultrasonics, Ferroelectrics, and Frequency Control* **55**(1), pp. 208-213 (2008).

IV S. Härmä, W. G. Arthur, C. S. Hartmann, R. G. Maev, and V. P. Plessky, "Inline SAW RFID tag using time position and phase encoding", *IEEE Transactions on Ultrasonics, Ferroelectrics, and Frequency Control* **55**(8), pp. 1840-1846 (2008).

V S. Härmä, V. P. Plessky, X. Li, and P. Hartogh, "Feasibility of ultra-wideband SAW RFID tags meeting FCC rules", *IEEE Transactions on Ultrasonics, Ferroelectrics, and Frequency Control*, accepted for publication.

Throughout the overview, these publications are referred to by their Roman numerals.

Author's Contribution

This dissertation is a result of the work carried out in the Materials Physics Laboratory, in the Laboratory of Optics and Molecular Materials, and in the Department of Applied Physics at the Helsinki University of Technology (TKK), Finland, during the years 2004-2008.

All Papers were prepared in collaboration with Victor P. Plessky (GVR Trade SA, Bevaix, Switzerland). Paper I involved cooperation with EFTECH Co. Ltd. (Cheongwon, Chungbuk, South Korea) and the University of Ulsan (Ulsan, South Korea). Papers III and IV were coauthored by Clinton S. Hartmann (RF SAW Inc., Richardson, Texas, USA) and involved collaboration with Temex (Sophia-Antipolis, France). Paper IV was prepared in cooperation with the Department of Physics at the University of Windsor (Windsor, Ontario, Canada) and Paper V is the result of collaboration with the Max Planck Institute for Solar System Research (Katlenburg-Lindau, Germany).

The author played a key role in all the research presented in Papers I-V. She had the main responsibility for the design of the devices studied in Papers II-V. She carried out all the simulations and the analyses of the simulated and experimental data reported in this dissertation. She performed a significant main part of the programming related to the data analysis and extracted all the results. All the papers were written mainly by her. The author presented the essential results of Paper I in the 2007 IEEE MTT-S International Microwave Symposium and those of Papers III-V in the annual IEEE International Ultrasonics Symposia of 2006-2008.

List of Abbreviations

The following abbreviations are used in the overview:

BEM	boundary element method
BPSK	binary phase shift keying
COM	coupling of modes
DART	distributed acoustic reflection transducer
DDL	dispersive delay line
EM	electromagnetic
EWC	electrode-width-controlled
FCC	Federal Communications Commission
FEM	finite element method
FEUDT	floating-electrode unidirectional transducer
FFT	fast Fourier transform
IC	integrated circuit
IDT	interdigital transducer
ILRAC	inline reflective array compressor
ISM	industrial, scientific, and medical
LFM	linear frequency modulated
MPGK	multiple pulse per group keying
MSC	multistrip coupler
NSPUDT	natural single-phase unidirectional transducer
PPM	pulse position modulation
PTSK	phase and time shift keying
RAC	reflective array compressor
RFID	radio-frequency identification
RSPUDT	resonant single-phase unidirectional transducer
SAW	surface acoustic wave
SPUDT	single-phase unidirectional transducer
SRAC	slanted reflective array compressor
TCD	temperature coefficient of delay
UWB	ultra-wideband

Contents

1   Introduction

Radio-frequency identification (RFID) [1, 2] has already existed for several decades but it has only recently come into public awareness as an efficient way of labeling and identifying objects, people, and animals. The principal advantage of RFID over the more traditional barcode labeling [3–5] is that it is read using a radio signal. Hence, an unobstructed line-of-sight is not needed between the reader and the label. In addition, RFID labels, or tags, can carry a significantly larger amount of information than barcodes. They also are physically robust whereas printed barcodes can easily be smudged or damaged. Furthermore, it is possible to read many RFID tags simultaneously [6–10] and the presence of a human operator is generally not needed.

RFID has numerous applications. It is used, for example, in building access control [11], production logistics [12–14], supply chain and inventory management [15–17], collecting of road tolls [18, 19], ticketing of passengers in transportation systems [20], automatic sorting of luggage at airports and of parcels at postal services [21–23], and prevention of thefts in shops and libraries [24, 25]. Recently, it has also been tested as an identification method to be used for asset tracking aboard the International Space Station [10].

RFID tags typically are powered integrated circuits (ICs) containing a computer microchip. They basically fall into two categories depending on their source of electrical power. While active tags usually have an on-board battery, passive tags power their circuitry by using a part of the interrogation signal energy transmitted by an external reader. This thesis focuses on a type of RFID tag that is even more passive than the passive IC tag. It does not contain an integrated circuit nor a computer microchip but relies on surface acoustic wave (SAW) technology. SAW RFID tags are linear passive devices whose operation does not require a threshold energy. They employ SAW delay lines and simply reflect the interrogation signal back in a form modified according to the identification information stored on the tag. SAW tags [26] generate a response at any power level, usually orders of magnitude lower than what is required for IC tags. In general, SAW technology lends itself well to the production of RFID tags: SAW devices can combine long delay times with a small device size. They also have a simple structure and can achieve low losses.

1.1   Surface Acoustic Wave RFID Tags

The fundamental physical phenomenon lying behind surface acoustic wave devices is piezoelectricity [27, 28]. This is, in general terms, a coupling between a material's electrical and mechanical properties: in certain dielectric crystals, the application of
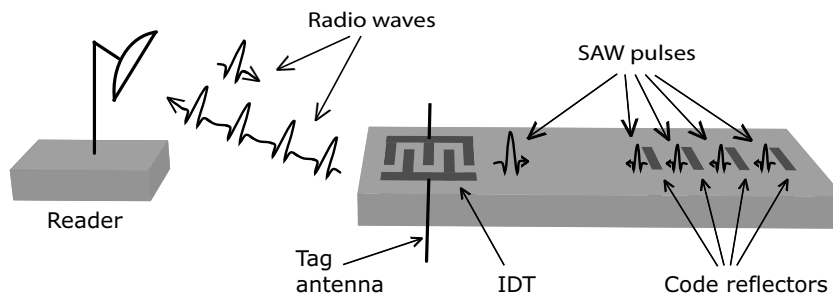
Figure 1.1: Operating principle of a SAW RFID tag.

mechanical stress produces an electric polarization and, conversely, such a crystal undergoes a mechanical distortion when an electric field is applied. This property is used in many applications to produce a mechanical output from an electrical input or vice versa. In SAW devices, the transduction between an electrical signal and an acoustic wave is achieved by utilizing an interdigital transducer (IDT) [29], consisting of two interlaced comb-like metal structures deposited on the surface of a piezoelectric substrate.

The operation principle of a SAW RFID tag is illustrated in Fig. 1.1, which schematically depicts the reader and the essential parts of the tag, that is, the substrate and the metal structures. As usual, RFID is based on radio communication between the reader unit and the tag. The reader sends an interrogation signal which is received by the tag, delayed and modified within the tag according to the stored identification information, and finally retransmitted for the reader to detect and process. More specifically, once received by the tag antenna, the interrogation signal is converted into a surface acoustic wave by an IDT. The generated wave propagates along the surface of the substrate and is partly reflected and partly transmitted at precisely positioned reflectors, consisting of narrow metal strips. Finally, the reflected train of SAW pulses carries a code based on the delays of individual reflections or, in other words, on the positions of the reflectors. The encoded acoustic signal is reconverted into electric form by the IDT and transmitted by the antenna to the reader.

1.1.1 SAW Tag Device Geometries

SAW identification tags generally consist of two parts: first, an IDT, for generating and receiving SAW pulses, (or several IDTs if the tag input and output are separated) and, second, a means for modifying (encoding) the interrogation signal before retransmitting it. The earliest SAW tags had an input IDT and several output IDTs as shown

in Fig. 1.2a. The input IDT and all output IDTs were arranged in-line and connected to common busbars [30, 31]. The group of output IDTs was spatially separated from the input IDT, hence providing an initial delay for distinguishing the transmitter and clutter energy from the reply energy. The drawback of this arrangement is that the output transducers also act as launch transducers as well as partial reflectors of SAWs. Spurious responses are thus created when SAWs launched or reflected by the various encoding transducers are picked up by other transducers.

In improved geometries, the output transducers were distributed into several parallel acoustic channels [32–34], as depicted in Fig. 1.2b. However, such multichannel geometries use more space in the transverse direction and have increased losses. A suggested improvement, sketched in Fig. 1.2c, brought the encoding elements back in one common acoustic channel by replacing the encoding output IDTs with an array of chevron-type reflectors [34, 35]. With the slanted chevron reflectors, multiple reflections between encoding elements could be avoided. This configuration already relied on the invention of replacing the encoding transducers with acoustic wave reflectors [35, 36]. Using reflectors instead of transducers enabled a more efficient use of the substrate area. As shown in Fig. 1.1, the waves could now make a round trip from the IDT to the reflectors and back. In the scheme depicted in Fig. 1.1, the same IDT is used for both input and output. A further reduction of tag length can be obtained by folding the acoustic channel into, for example, a U-path using track-changing structures [37] or inclined reflectors [38], as illustrated in Fig. 1.2d. In Paper III, the acoustic channel is folded into a Z-path using two strongly reflecting inclined reflectors.

Previously reported SAW tag designs use standard bidirectional transducers that generate wave propagation equally into the two directions perpendicular to the interdigital electrodes [34, 39]. For such tags, code reflectors have to be placed on both sides of the IDT. Otherwise, as is the case for the tags depicted in Fig. 1.2, the device will inherently have a bidirectionality loss of -3 dB both at generation and reception of SAWs. However, arranging the reflectors on both sides of the IDT results in a relatively large tag size as free surface must be provided between the IDT and the reflectors on the two sides. A unidirectional IDT would generate wave propagation predominantly in one direction. Then all reflectors could be placed on one side of the transducer without the burden of bidirectionality loss.

1.1.2 Unidirectional Transducers

Figure 1.3 schematically depicts a few of the early unidirectional transducers. The configuration (a) [40–42] includes two collinear bidirectional IDTs separated by a distance $\lambda/4$. Unidirectionality is achieved by driving the two transducers in phase quadra-

(a) input IDT output IDTs

(b) input IDT output IDTs

(c) input IDT chevron-type code reflectors

output IDT

(d) input/output IDT inclined reflectors
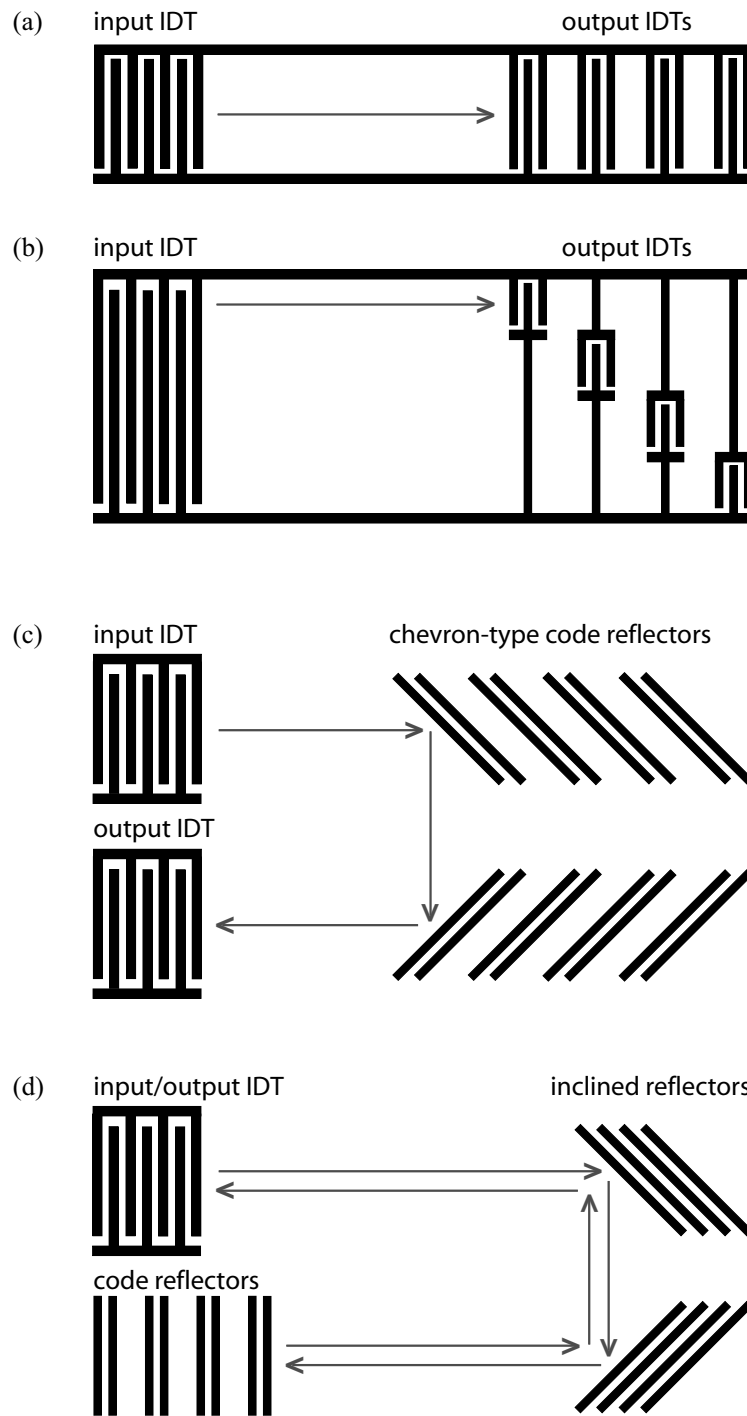
code reflectors

Figure 1.2: Tag geometries. The arrows indicate the SAW propagation path. (a) Input IDT and several output IDTs. (b) Multiple parallel acoustic channels. (c) Chevron-type code reflectors. (d) U-shaped acoustic channel.
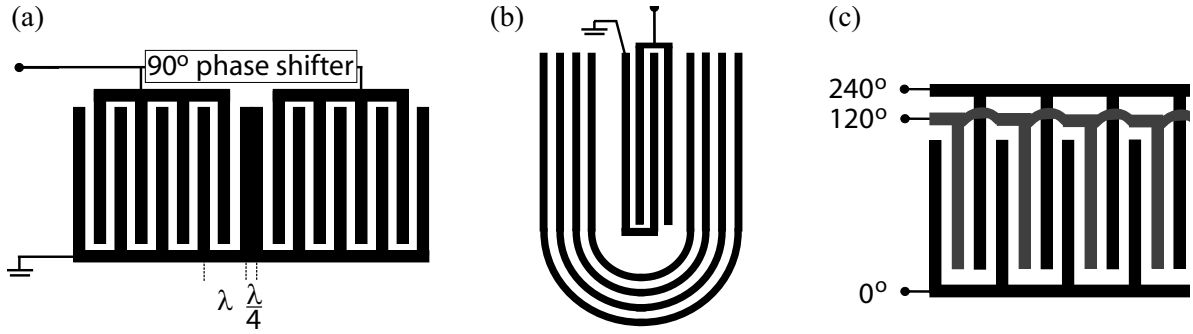
Figure 1.3: Early unidirectional transducers (with forward direction to the right). (a) Two collinear IDTs driven in phase quadrature. (b) Multistrip coupler unidirectional transducer. (c) Three-phase unidirectional transducer.

ture. However, this device inherently has a limited bandwidth. The approach (b) [43] is constructed by placing a bidirectional IDT within a U-shaped multistrip coupler (MSC) [44, 45] such that the IDT is displaced from the center of the U by a distance $\lambda/8$. This arrangement provides an improvement in bandwidth but has other drawbacks. It requires a relatively large chip area and is impractical for substrates with low piezoelectric coupling. The arrangement (c) is the so-called three-phase unidirectional transducer [46, 47] that uses three sets of interdigital electrodes driven 120° out of phase. This is a more compact configuration but involves multilayer manufacturing techniques.

An important innovation in the area was the single-phase unidirectional transducer (SPUDT) [48]. As shown in Fig. 1.4a, it comprises a conventional split-finger IDT with a second metal layer on alternate electrodes to provide a superimposed reflector array. The SPUDT operation relies on internal reflections within the transducer, through which unidirectionality is achieved by displacing the centers of wave excitation a distance $\lambda/8$ from the centers of reflection. Further developments of this device eliminated the second metallization step by placing reflector banks in spaces between transducer sections [49, 50] (Fig. 1.4b) or by replacing every second transducer electrode of a split-finger configuration with a floating electrode, thus creating the floating-electrode unidirectional transducer (FEUDT) [51, 52] (Fig. 1.4c). Other SPUDT designs, such as the distributed acoustic reflection transducer (DART) [53] (Fig. 1.4d) and the electrode-width-controlled SPUDT (EWC/SPUDT) [54] (Fig. 1.4e) emerged to meet the requirement on enhanced control of reflectivity inside the transducer structure. It was also discovered that with special asymmetric crystal orientations, a standard symmetric
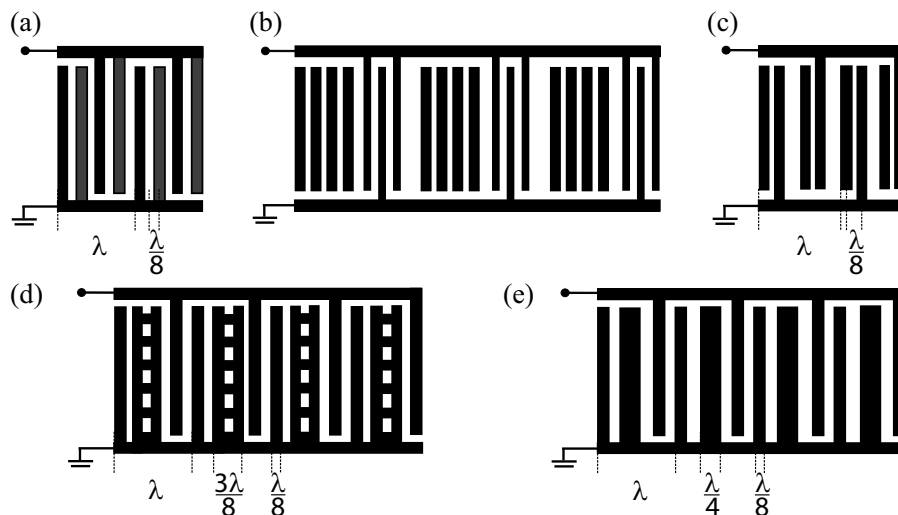
Figure 1.4: (a) Single-phase unidirectional transducer (SPUDT). (b) Group-type unidirectional transducer. (c) Floating-electrode unidirectional transducer (FEUDT). (d) Distributed acoustic reflection transducer (DART). (e) Electrode-width-controlled SPUDT (EWC/SPUDT).

IDT exhibits unidirectionality. The device relying on this phenomenon is called the natural SPUDT (NSPUDT) [55]. A later important development in the field of unidirectional transducers was the resonant SPUDT (RSPUDT) [56]. It combines regions with forward and backward unidirectionality such that resonant acoustic cavities are formed but overall unidirectionality is maintained.

The majority of the SPUDT designs mentioned above have the disadvantage of a small critical dimension. Linewidths of $\lambda/8$ are common among them but beyond the large-scale fabrication techniques for frequencies well above 1 GHz. SPUDT structures were taken to the 2-GHz range by employing $\lambda/4$-wide (and wider) electrodes [57–61].

The possibility to use a unidirectional transducer in SAW identification tags has been mentioned by several authors [35, 37, 60, 62, 63] but without a further description of tag design and experimental verification. Section 3.1.2 of this thesis describes a 2.45-GHz SPUDT design and Papers III and IV present experimental results for tags employing this transducer.

1.1.3 Encoding Methods

The encoding of the first SAW identification tags (with an input IDT and an array of output IDTs, as shown in Fig. 1.2a) was based on amplitude modulation, more

specifically, on on/off-keying [30,64]. The positions for output transducers were equally spaced throughout the array. The presence of an output IDT within its designated slot signified a logic 1, while an absent output IDT represented a logic 0. Another suggested implementation of on/off-keying involved having all output IDTs present and placing rubber pads in the spaces between them [32,65]. By applying pressure on one of the pads, it was possible to disrupt the transmission of SAW to the region distal to the stressed pad. However, this scheme yielded a very limited code space.

Another implementation of binary coding was through phase modulation. An example of using binary phase shift keying (BPSK) involved two tracks connected electrically in parallel [66]. Each track had an input transducer and an array of output transducers. The output transducers were placed at equal delays from the input transducers in the two tracks. However, the electrode polarities were opposite in the two channels. BPSK, that is, a phase shift of either $0°$ or $180°$, was achieved through disconnection of an output transducer in either track at each bit position.

A further development of phase encoding for the single-track tag design of Fig. 1.2a was presented in [67]. In this configuration, all output transducers were present and equally spaced. The code signals were delayed using 0, 1, 2, or 3 so-called delay pads deposited in regions between the output transducers in order to provide a phase shift of $90°$ per pad. While the number of different code sequences obtainable with the basic on/off-keying was 2^n, where n is the number of output transducers, the above described phase encoding yielded 4^n different codes.

In general, the phases of the response signals are sensitive to changes in temperature, especially for lithium niobate (LiNbO$_3$) substrates that feature a high temperature coefficient of delay (TCD) defined as [68]

$$\text{TCD} = \frac{1}{\tau_0}\frac{\tau - \tau_0}{\vartheta - \vartheta_0},\tag{1.1}$$

where τ refers to time delay and ϑ to temperature. The subscript 0 stands for reference values. The 128°-LiNbO$_3$ and YZ-LiNbO$_3$ substrates have TCDs of 75 ppm/°C and 94 ppm/°C, respectively [69]. At 2.45 GHz, these coefficients correspond to the respective phase errors of about $66°/(°C·\mu s)$ and $83°/(°C·\mu s)$.

To simplify the calibration process, an encoding method based on the time delays (or time positions) of response signals was proposed [34,38]. In time position encoding, each pulse occupies a slot of width Δt_{slot}. To avoid intersymbol interference, the slot width is made roughly equal to the time-width of the pulses, approximately $1/B_{\text{syst}}$, where B_{syst} is the system bandwidth. These slots form N_g groups of N_s slots. In the simplest scheme, which is also known as the conventional pulse position modulation (PPM), only one slot within a group is occupied by a pulse. In this case, the number of

groups N_g also gives the number of code reflectors on the tag. The number of different code sequences obtainable through this method is $N_s^{N_g}$.

To enhance data capacity, it was suggested to use time slots much narrower than $\Delta t_{\text{slot}} = 1/B_{\text{syst}}$ while keeping the total delay of a group unchanged. Slot widths of $\Delta t_{\text{slot}}/5$ or $\Delta t_{\text{slot}}/10$ were proposed for increasing the number of possible pulse positions within a group. As discrimination between adjacent pulse positions is very poor with such slot widths, a small increment or decrement of distance was added between subsequent pulse positions to provide a phase step of, for example, $\pm 90°$. In this phase and time shift keying (PTSK), a certain fixed phase was assigned to each possible pulse position. It is to be noted that in this method, phase shift keying was used so as to ensure a correct interpretation of pulse position data rather than to perform simultaneous and independent time position and phase encoding, as is the case in Section 3.3 and in Paper IV. Another improvement to PPM was the multiple pulse per group keying (MPGK) where the slot width was kept at Δt_{slot} but more than one pulse per group was allowed. This method provided $\binom{N_s}{N_p}$ different codes per group, where N_p denotes the number of pulses per group. A combination of PTSK and MPGK yielded a significant enhancement of data capacity. Pulse overlapping due to narrow slots was avoided either by imposing a minimum pulse spacing rule that gave the number of slots to be skipped between pulses or by using the slot orthogonality with phase shifts of $\pm 90°$, as described above. PTSK, MPGK, and their combination were proposed in [63, 70, 71].

1.1.4 Ultra-Wideband Radio Technology and SAW Devices

The currently emerging ultra-wideband (UWB) radio technology enables short-range communications with high speed and low power [72]. The principle of this technology is to reuse an already occupied frequency spectrum but with very low power and without causing interference to existing radio services. Regulation for the use of UWB technology has already been fixed or is currently under way in many countries [73–77]. According to the Federal Communications Commission (FCC), which is the regulatory authority in the United States, an UWB device is a device emitting signals with a fractional bandwidth greater than 20% or a bandwidth of at least 500 MHz.

The use of wideband (spread spectrum) and UWB signals in SAW sensors and SAW-device-based communication systems has been shown to enable robust data transmission even in very noisy radio environments. This has been achieved through matched-filter operation using chirp signals [78–84] or other modulated waveforms [85–88]. A UWB SAW correlator operating within the FCC [73–75] designated band for developmental UWB communication devices was recently demonstrated [86]. However, the possibility of using UWB signals in surface acoustic wave identification tags has

not yet been addressed in detail in the literature, although the use of spread spectrum signals for tags has been discussed in a few publications [89–94]. Meanwhile, this possibility is especially attractive because, for SAW tags, the used frequency band B is of primary importance. According to Shannon's equation [95], the number of different codes that can be obtained (when the signal-to-noise ratio is 1) is determined by the product BT, where T is the coding time duration. As the coding time duration is normally limited to 2 μs to 4 μs in SAW devices due to high propagation losses at GHz-frequencies, the availability of wide frequency bands is a clear benefit when a large information capacity is desired. Or, if the enhancement of data capacity is not necessary, ultra-wide bands can be exploited to drastically shorten the coding time duration and hence to reduce the tag size. A design for such a UWB SAW tag is proposed in Paper V.

1.1.5   Properties of Metal Reflectors

To achieve a reasonably high data capacity, a SAW tag must include around 50 reflecting electrodes (in groups of one or a few electrodes). Such a large number of electrodes implies that the reflectors in the beginning of the reflective array must have very weak reflectivities. As discussed in Paper I, this can be achieved by using narrow open-circuited aluminum electrodes. Their reflectivity can be controlled by varying their width. In addition to being useful for SAW tags, the weak and controllable reflectivity of narrow electrodes also offers advances for the design of dispersive delay lines (DDLs), which are devices imposing different time delays on the different spectral components of an input signal.

The first SAW DDLs, depicted in Fig. 1.5a, consisted of dispersive IDTs (or chirp IDTs) [96]. The electrode pitch of these transducers was gradually increased or decreased in order to yield a linear frequency modulated (LFM) impulse response. (This type of IDT can also be used in SAW tags to provide a means for signal processing within the tag, as discussed in Section 3.4 and in Paper V.) However, these transducer-type DDLs suffered from spurious signals and were soon replaced by the reflective array compressor (RAC) [97–99]. The RAC consists of two acoustic tracks coupled together. As sketched in Fig. 1.5b, one track of a RAC has a short input IDT and an array of slanted grooves acting as wave reflectors. The other track has a groove array that is a mirror image of the first one and a short output transducer. The groove spacing is increased with distance from the IDTs. Both groove arrays reflect the incident SAWs at an angle of 90° in the region where the grating periodicity matches the SAW wavelength and a U-shaped acoustic channel is formed.

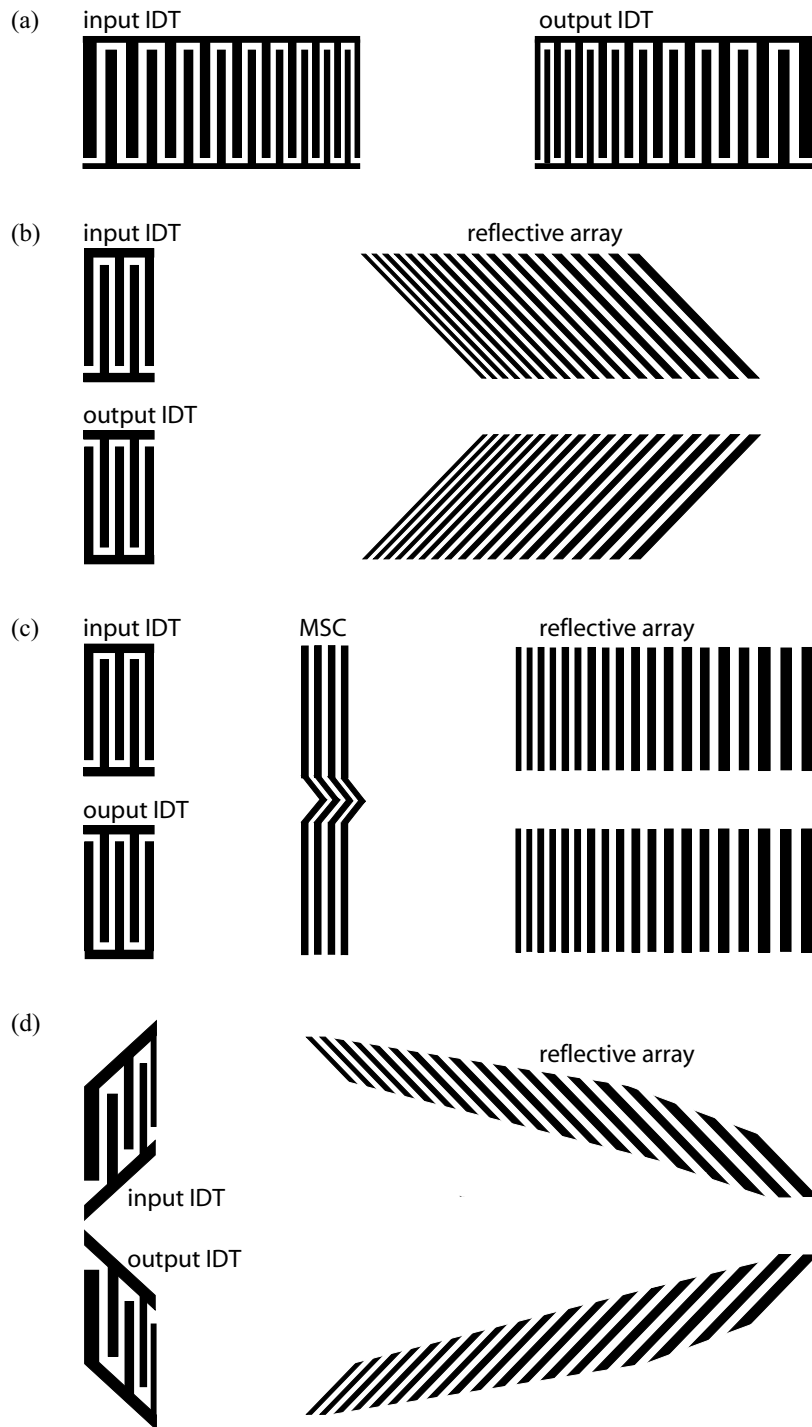Although the RAC had many advantages over its predecessor (such as a low level of

- 10 -

Figure 1.5: Dispersive delay lines. (a) IDT-type DDL. (b) Reflective array compressor (RAC). (c) Inline reflective array compressor (ILRAC). (d) Slanted reflective array compressor (SRAC).

spurious modes and of multiple reflections, a higher tolerance of defects, and a folded acoustic path that doubles the dispersion time for a given substrate length), its fabrication involved a complicated and time-consuming process: the transducer metal was deposited in one step and the grooves were ion-beam-etched one by one in another step. The reflectivity of the grooves was determined by their depth, which was controlled by the etching time. In addition, precise alignment was needed between the transducers and the groove arrays. Another drawback of the RAC was its sensitivity to variations of temperature. Changes in temperature introduced changes in delays and in reflection angles.

A single-stage fabrication process was provided by replacing grooves either with arrays of metal dots [100–102], whose reflectivity was controlled by the dot size and density, or with metal strips [103–105], for which reflectivity was controlled by either reflector length or width. Further developments of DDLs included the inline reflective array compressor (ILRAC) where the reflector arrays (grooves, dots, or metal strips) were oriented parallel to the input and output IDTs [106–108], as shown in Fig. 1.5c. With this geometry, a reduction in insertion loss was achieved as two reflections of 90° were replaced by a single reflection of 180°. The design was also simplified since the velocity and scattering anisotropy needed not to be considered. Configurations aiming at a reduction of interelectrode reflections, present in both RACs and ILRACs and degrading the delay line performance, were also proposed. The slanted reflective array compressor (SRAC) [109,110], schematically shown in Fig. 1.5d, combines slanted input and output transducers with slanted reflector arrays. In this device, different frequency portions have their own acoustic channels and need not travel long distances under an electrode structure with a non-matching periodicity. An alternative for slanted transducers is offered by the fan-shaped transducer whose electrode pitch changes linearly along the aperture [110].

In the days of intensive development of RACs, metal strips did not yet present a valid alternative to grooves at frequencies of several hundred megahertz due to linewidth limitations. Because of this and the intricacy of the fabrication process, DDLs have remained expensive and been produced on a piece-by-piece basis. However, at present, there is a renewed interest [111] to use DDLs in, e.g., UWB communication systems. Modern standard photolithography also allows for the manufacturing of metal strips with a width of about 0.4 μm, sufficiently narrow to provide the weak reflectivity needed in metal RACs.

Although a few early papers [112–116] present some fragmentary data on the reflectivity of aluminum electrodes on YZ-LiNbO$_3$, a substrate frequently used for DDLs due to its reduced diffraction effects [117], comprehensive and easily accessible data are

unavailable. In Paper I, the reflectivity and SAW attenuation within reflector gratings consisting of open-circuited aluminum electrodes are determined. For the design of SAW tags, precise knowledge of reflector parameters is crucially important. The full set of reflection, transmission, and scattering parameters must be known. Moreover, in order to be able to control the amplitudes of tag response signals and to use phase-based encoding reliably, the parameters related to reflection and transmission must be known as a function of frequency. A series of investigations [118–120] has previously been carried out to determine the reflection and scattering parameters of short reflectors on 128°-LiNbO$_3$ but without frequency-dependence. As a response, a method for calculating the frequency-dependent parameters was recently developed [121] but involves heavy calculation. Section 2.2 and Paper II present a simplified method for the extraction of frequency-dependent reflector parameters. It is based on the S parameter data of a tag test device and does not require any specialized software.

1.2   Scope of This Thesis

SAW RFID tags provide many intrinsic advantages over the market-dominating semi-conductor-based RFID tags. SAW tags are totally passive devices and can be interrogated using low-power readers. Their simple structure, a single-layer metal pattern deposited on a piezoelectric substrate, can be accomplished by means of standard photolithography. However, the final commercial breakthrough of SAW tags has not yet occurred. SAW tags have been criticized for being of too large a size, too expensive, and not having enough data capacity. The aim of this work has been to investigate whether SAW tags can be made a valid competitor for semiconductor-based tags, and to create new tag designs to justify an affirmative answer to this question. The design and analysis of SAW tag devices have been carried out using results of simulations and measurements. Compact device geometries have been searched for and solutions for combining time position encoding and phase encoding have been tested. The feasibility of UWB SAW tags has been studied through simulations and experiments. Furthermore, the frequency-dependent reflection, transmission, and scattering parameters for short metal reflectors have been determined in order to achieve accurate tag designs with reliable coding.

This research mainly limits itself to the level of the SAW tag device. It focuses on the operation of the entity formed by the piezoelectric substrate, transducers, and reflectors. Antenna and reader technologies fall outside the scope of the present work.

2   Extraction of Reflector Parameters

Precise knowledge of reflector properties is one of the prerequisites for accurate tag designs. The parameters related to reflection, transmission, and scattering of surface acoustic waves at metal electrodes are needed for the control of amplitudes and phases of tag response signals. Otherwise, it is difficult to achieve reliable identification.

This thesis work includes two parts of parameter extraction: First, the reflectivity and SAW attenuation within reflector gratings consisting of narrow metal strips on YZ-LiNbO$_3$ are determined. Second, a method for extracting the reflection, transmission, and scattering parameters of short metal reflectors from test device S parameter data is developed. In both parts, parameter extraction relies on the analysis of simulated and experimental S parameters. The simulated data are obtained using software based on the combined finite- and boundary element method (FEM/BEM) [122, 123]. This method is widely used for the analysis of SAW devices. FEM is well-suited for describing the electrodes and the semi-infinite substrate is treated using BEM with Green's function formalism [123, 124]. The FEM/BEM simulator uses the material constants for LiNbO$_3$ determined in [125]. For an n-port device, the software calculates a sequence of Y parameter matrices, one complex-valued $n \times n$ matrix for each frequency point. The frequency range B_W of the simulation and the frequency step Δf are user-defined. These determine the width of the time window T_W and the time resolution Δt obtained when inverse Fourier transform is used for producing the time response. The parameters T_W and Δt are given by

$$T_W \;\; = \;\; \frac{1}{\Delta f} \tag{2.1}$$

$$\Delta t \;\; = \;\; \frac{1}{B_W}. \tag{2.2}$$

The Y parameters are readily transformable to S parameters [126], which form the basis of almost all analysis presented in this work.

2.1   Reflectivity and Attenuation of Narrow Electrodes

Reflectors with weak reflectivity, consisting of narrow metal strips, are needed both in SAW tags and in DDLs. In Paper I, the reflectivity per wavelength $|\kappa\lambda_0|$ and the SAW attenuation per wavelength $\gamma\lambda_0$ within gratings of metal electrodes are determined. The reflectivity $|\kappa\lambda_0|$ gives the ratio of the wave amplitude reflected within a distance of one acoustic wavelength to the incident wave amplitude. The acoustic wavelength is defined as $\lambda_0 = v/f_0$, where v is the free-surface SAW velocity on the
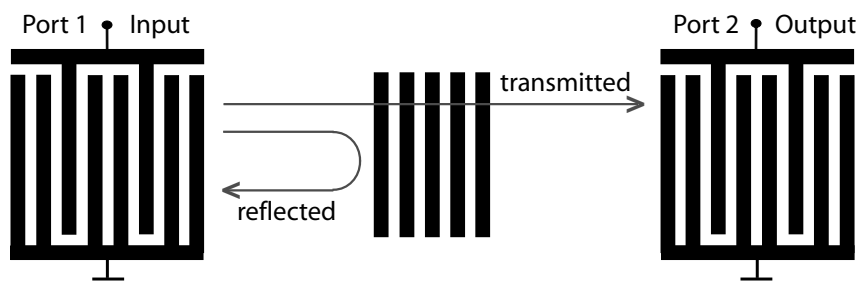
Figure 2.1: Schematic drawing of the test structure used in the extraction of reflectivity $|\kappa\lambda_0|$ and attenuation $\gamma\lambda_0$. The IDTs are identical and have three electrodes per wavelength. They are located symmetrically on the two sides of the studied reflector.

given substrate and f_0 is the SAW frequency. The attenuation $\gamma\lambda_0$ is used as a measure of wave damping due to propagation under metal structures. It usually has the unit dB/λ_0 or Np/λ_0 (Np stands for neper, 1 Np = 8.686 dB). As the test structures used in this work involve fundamental-mode reflectors, that is, the electrode spacing within reflectors is $\lambda_0/2$, the results obtained for $|\kappa\lambda_0|$ and $\gamma\lambda_0$ are per two electrodes.

2.1.1   Simulations and Experiments

The test structure used in the extraction of $|\kappa\lambda_0|$ and $\gamma\lambda_0$ is schematically depicted in Fig. 2.1. It is a 2-port device with two identical IDTs and a reflector. The reflector is placed halfway between the IDTs and comprises 49 open-circuited electrodes. The IDTs have three electrodes per wavelength and operate at a center frequency of 201 MHz. This type of IDT has lower reflectivity than a standard IDT, which is a useful feature reducing parasitic signals. The substrate material is YZ-LiNbO$_3$, which is especially suitable for long structures, such as SAW tags and DDLs, due to its reduced diffraction effects. For the reflectors to be analyzed, the metal ratio m/p (where m is the electrode width and p is the electrode pitch, that is, the center-to-center distance between neighboring electrodes) is varied from 0.2 to 0.5 from one test structure variant to another. The test structures are simulated using FEM/BEM software and experimental data are obtained through network analyzer measurements on fabricated devices.

2.1.2   Analysis

Reflectivity and attenuation are extracted using the ratio of amplitude reflection and transmission coefficients, R/T. The use of this ratio was suggested in [127] for extract-
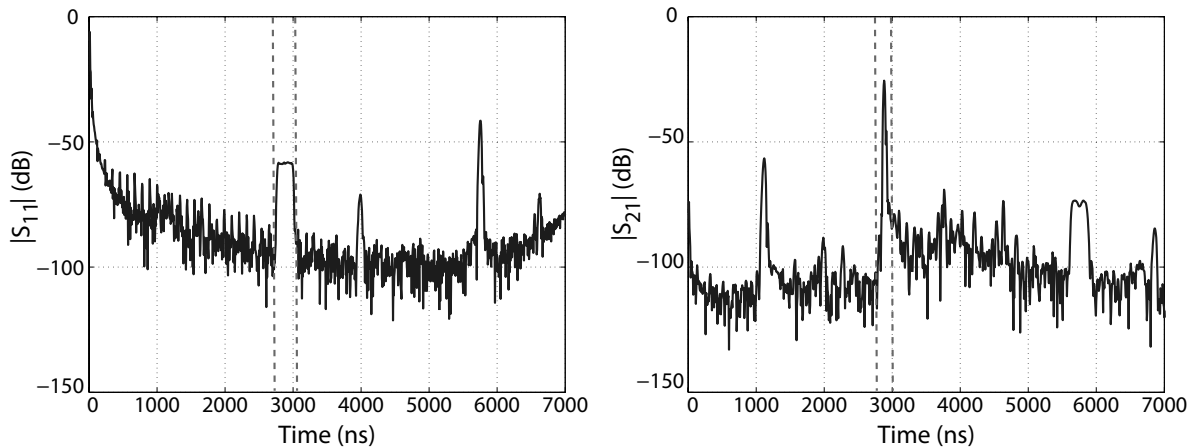
Figure 2.2: Experimental data for the structure of Fig. 2.1. *Left:* $|S_{11}|$ in the time domain. The reflected signal is between the dashed lines. *Right:* $|S_{21}|$ in the time domain. The transmitted signal is between the dashed lines.

ing reflectivity under a SPUDT. For the structure shown in Fig. 2.1, R/T is obtained by a time-gating method similar to that used in [114]. This is done by first transforming the S_{11} and S_{21} parameters to the time domain using the (inverse) fast Fourier transform (FFT) [128]. Then the reflected signal (with the path input IDT $\rightarrow$ reflector $\rightarrow$ input IDT) is separated from the rest of the S_{11} data and the direct propagation signal (with the path input IDT $\rightarrow$ reflector $\rightarrow$ output IDT) is time-gated from the S_{21} data, as indicated with dashed lines in Fig. 2.2. The ratio S_{11}/S_{21} of the time-gated signals is calculated after transformation back to the frequency domain. Figure 2.3 shows the time-gated signals separately (left) and the ratio of these two signals (right) as a function of frequency. The IDT performance and the propagation loss have equal contributions in both signals and are cancelled when the ratio is calculated. Therefore, S_{11}/S_{21} of the time-gated signals is in fact equivalent to the R/T of the reflector.

The reflectivity per wavelength $|\kappa\lambda_0|$ can be derived from the coupling-of-modes (COM) [129, 130] equations for reflection and transmission coefficients as [131]

$$|\kappa\lambda_0| = \frac{\lambda_0}{L}\mathrm{asinh}\left|\frac{R(f_c)}{T(f_c)}\right|, \tag{2.3}$$

where λ_0 is the wavelength of the reflector structure, f_c its center frequency, and L the reflector length ($L = N_{el}p$, where N_{el} is the number of reflector electrodes and $p = \lambda_0/2$ the pitch of the electrodes). The SAW attenuation $\gamma\lambda_0$ (in Np/λ_0) within
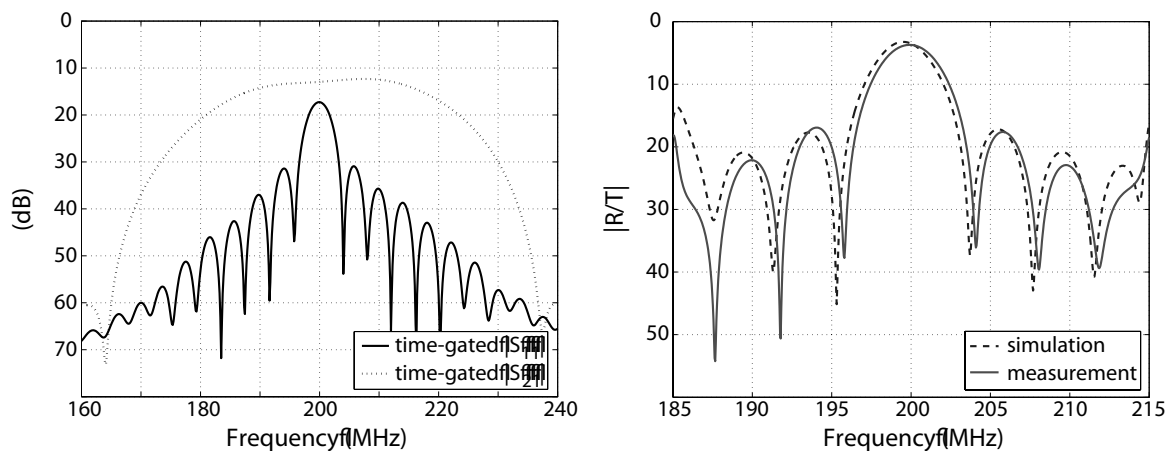
Figure 2.3: *Left:* Time-gated $|S_{11}|$ and $|S_{21}|$ for the structure of Fig. 2.1 in the frequency domain. Experimental data. *Right:* Simulated and experimental $|R/T|$ ratio.

the grating is given by

$$\gamma\lambda_0 = \frac{4n^2\pi \left|\frac{R(f_{\pm n})}{T(f_{\pm n})}\right|}{\left|\frac{\Delta f_n}{f_c}\right| (N_{\text{el}} - 1)^3 |\kappa\lambda_0|}, \tag{2.4}$$

which directly relates the depth of the notches in the R/T curve to wave attenuation. In Eq. (2.4), f_n is the position of the nth notch, as counted from the main lobe, and

$$\frac{\Delta f_n}{f_c} = \frac{f_n - f_{-n}}{f_n + f_{-n}} \tag{2.5}$$

is the relative deviation of f_n from the center frequency of the grating [131]. In our case, $n = 1$ since we use the first notches around the center frequency. Plus and minus signs refer to the notches on the high- and low-frequency sides of the main lobe, respectively.

2.1.3 Results

In Paper I, it was estimated that for a typical high-BT DDL device ($B = 100$ MHz, $T = 50$ μs, and $f_c = 400$ MHz), the reflectivity of a single reflector electrode should be weaker than 0.3%. Experiments showed that for the narrowest electrodes tested ($m/p = 0.2$), reflectivities of 0.33% and 0.43% per λ_0 (per two electrodes) can be achieved for the relative metal thicknesses of $h/\lambda_0 = 1.15\%$ and 1.73%, respectively.
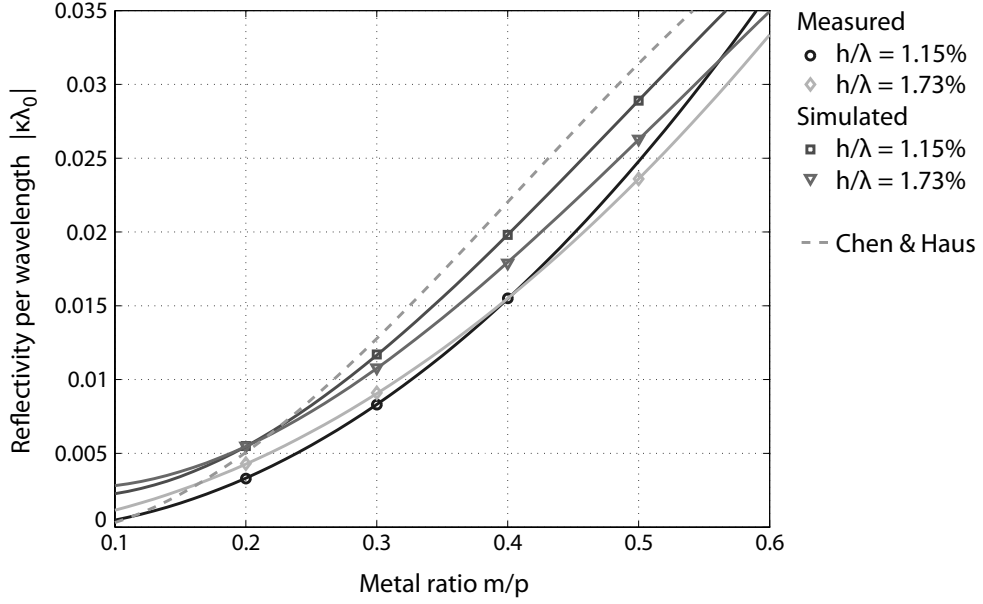
Figure 2.4: Extracted reflectivities of open-circuited aluminum electrodes on YZ-LiNbO₃. Results are compared to the theoretical data calculated by Chen and Haus [115], for which $h/\lambda = 1\%$.

Figure 2.4 shows the extracted reflectivities as a function of the metal ratio along with previously published theoretical values [115]. It is immediately seen that the reflectivity of open-circuited electrodes is smoothly - almost linearly - dependent on the metal ratio, which is very convenient for the control of reflectivity in DDLs and in SAW tags. The metal thicknesses used in the experiment were very small: only 1.15% and 1.73%. Therefore, reflectivity is mainly due to short-circuiting of the electric fields and not to mass-loading. The experimental reflectivities are systematically a bit lower than those simulated, which can be an indication of over-etched electrodes. This hypothesis is supported by the fact that the relative discrepancy is smaller for wide electrodes, for which the over-etch would be relatively less important.

The values of attenuation obtained in Paper I can only be considered fair estimates because the notch depth is easily influenced by the finite frequency step and, especially for the narrowest electrodes, by electromagnetic (EM) feedthrough. Due to the symmetry of the device, the reflected signal (input IDT → reflector → input IDT) and a signal propagating from the input IDT to the output IDT as EM feedthrough and back to the input IDT as a SAW are received at the same time and are not separable using time-gating. In simulations, a slightly asymmetric structure was used to separate these

two signals. In the experimental results, however, the signals are inseparable. Nevertheless, it is believed that for $m/p = 0.4$ and 0.5, attenuation is estimated correctly. In these cases, the obtained general level of attenuation is about $1 \cdot 10^{-3}$ to $2 \cdot 10^{-3}$ Np/λ_0.

2.2 Reflection, Transmission, and Scattering Parameters of Short Metal Reflectors

The second part of parameter extraction involves short metal gratings, that is, reflectors consisting of only one or a few open-circuited electrodes. These are used as code reflectors in SAW tags. As a reasonably large data capacity implies the use of a considerable number of code reflectors, the reflectors must have weak reflectivity and consist of only a few electrodes.

Previously, Lehtonen *et al.* [118–120] have done a series of investigations to determine the reflection and scattering parameters of reflectors consisting of 1 to 3 electrodes as a function of relative metal thickness (h/λ) and metal ratio (m/p). They have used test device Y parameters produced by a FEM/BEM-based simulator, obtained the impulse response through Fourier transformation, and used time-gating to separate the reflective echoes. However, their results do not give the parameter values as a function of frequency. The frequency-dependence of reflection, transmission, and scattering parameters has recently been studied by Wang *et al.* in [121]. They have developed a source regeneration method based on Green's function theory and FEM/BEM that directly calculates the reflection, transmission, and scattering parameters at each frequency point within a specified range of frequencies. Determining the parameters is faster this way but includes evaluation of the energy of scattered waves, which is difficult to accomplish experimentally.

Paper II reports an alternative method for determining the reflection, transmission, and scattering parameters of short metal reflectors as a function of frequency. This method takes the FEM/BEM-simulated or experimental S parameters of a test device as a starting point and analytically extracts the reflection and transmission coefficients (absolute values and phase angles) and the energy scattered into bulk.

2.2.1 Method

The test device is a primitive SAW tag having only three reflectors, as schematically depicted in Fig. 2.5. The IDT used for generation and reception of surface acoustic waves is of standard type and has 10 electrodes with alternating polarities. The three identical reflectors placed in the acoustic path each consist of a single floating electrode. The distances L_0, L_1, and L_2 (shown in Fig. 2.5) between the reflectors have been
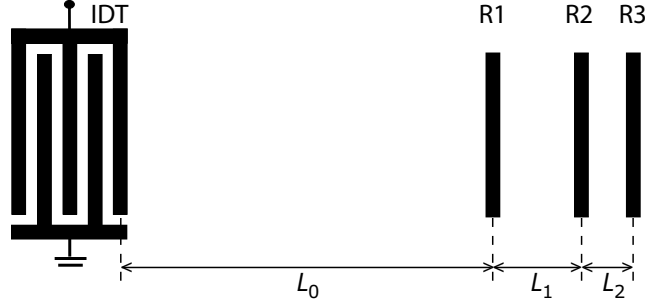
Figure 2.5: Schematic drawing of the test structure used for characterizing single-electrode reflectors. The reference planes for the distances L_0, L_1, and L_2 are located at the centers of the reflectors and at the center of the right-most IDT electrode.

chosen such that none of the first four reflections overlaps with any other reflection. The distance L_0 is measured from the center of the right-most electrode of the IDT to the center of the first reflector. The distances L_1 and L_2 are defined as the center-to-center distances of the first and second reflector (R1 and R2) and the second and third reflector (R2 and R3), respectively. The first three reflections originate from round-trip propagation between the IDT and the three reflectors, while the fourth one corresponds to the path IDT $\rightarrow$ R3 $\rightarrow$ R2 $\rightarrow$ R3 $\rightarrow$ IDT, that is, it involves multiple reflections between the second and third reflector.

A FEM/BEM simulation was carried out separately for the entire SAW tag structure described above and for a structure consisting of the IDT only. The S_{11} parameter of the IDT was then subtracted from the S_{11} parameter of the entire device. In this way, the data to be analyzed only contain the response of the reflectors and are clear of any contribution from the direct EM signal reflections from the IDT.

The frequency response of each reflection is separated from the total response using FFT and time-gating techniques. Figure 2.6 (left) shows the total response in the time domain. The first four reflections are indicated by dashed lines and numbered. After time-gating these signals, the time-gated data are transformed back to the frequency domain. Figure 2.6 (right) shows the time-gated S_{11} parameter for each of the four reflections of interest in the frequency domain. The ith reflection is denoted by S_i. The signals S_1, S_2, and S_3 overlap in Fig. 2.6 because propagation losses were assumed negligible in this numerical experiment.

The reflector parameters are directly extractable from the time-gated frequency responses S_i. The analysis also yields the free surface attenuation coefficient α and the
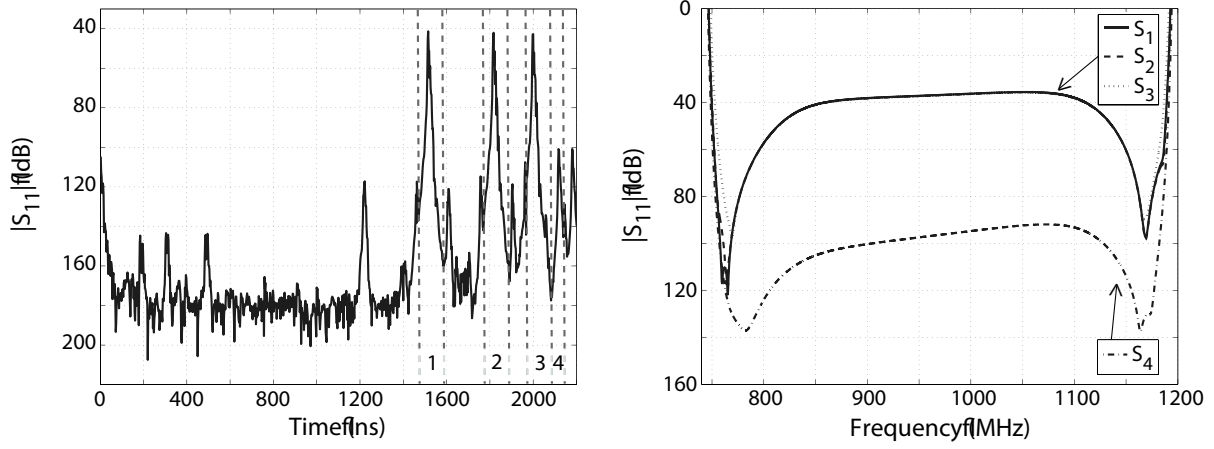
Figure 2.6: *Left:* $|S_{11}|$ of the 3-reflector SAW tag in the time domain and time-gating of the first four reflections. *Right:* Time-gated $|S_{11}|$ in the frequency domain for the four reflections of interest. The signals S_1, S_2, and S_3 overlap.

free surface wavenumber k. These are given by

$$\alpha = -\frac{1}{2(L_1 - L_2)} \ln \left| \frac{S_2^2}{S_1 S_3} \right| \tag{2.6}$$

and

$$k = -\frac{1}{2(L_1 - L_2)} \arg \left(\frac{S_2^2}{S_1 S_3} \right). \tag{2.7}$$

Writing the reflection and transmission coefficients as $R = re^{j\varphi_R}$ and $T = te^{j\varphi_T}$, respectively, their amplitudes and phases can be calculated from the following equations:

$$r = \sqrt{\left| \frac{S_4/S_2}{P_1^2} \right|} \tag{2.8}$$

$$t = \sqrt{\left| \frac{S_2/S_1}{P_1^2} \right|} \tag{2.9}$$

$$\varphi_R = \frac{1}{2} \arg \left(\frac{S_4/S_2}{P_1^2} \right) \tag{2.10}$$

$$\varphi_T = \frac{1}{2} \arg \left(\frac{S_2/S_1}{P_1^2} \right), \tag{2.11}$$

where $P_1 = e^{-\alpha L_1 - jkL_1}$ represents the propagation from the first reflector to the second reflector. The fraction of energy scattered into bulk is given by $E = 1 - r^2 - t^2$. In
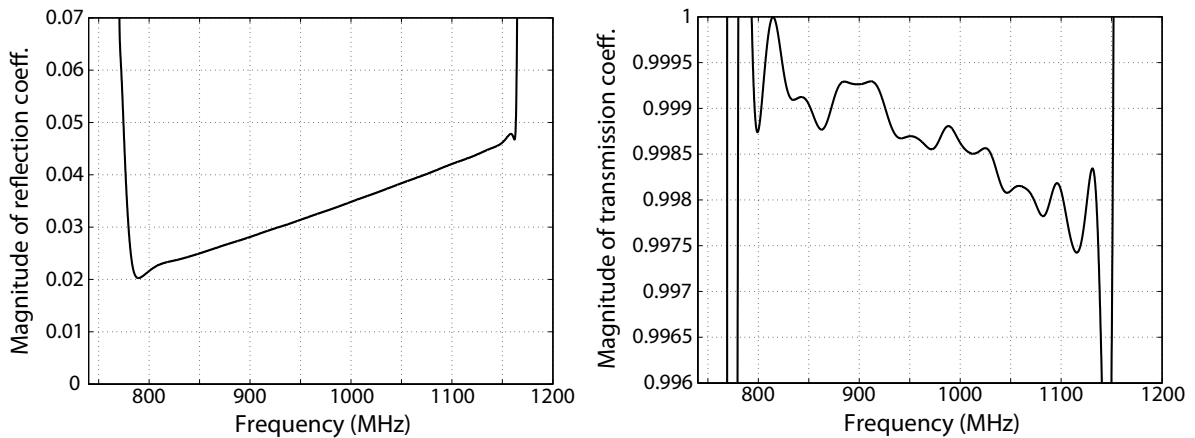
Figure 2.7: Frequency-dependent parameters for a single-electrode reflector on 128°-LiNbO$_3$ substrate ($h/\lambda = 2.5\%$ and electrode width is 0.8 μm). Extracted from simulated data. *Left:* Magnitude of the reflection coefficient. *Right:* Magnitude of the transmission coefficient.

Eqs (2.6) to (2.11), all multiplications and divisions are performed pointwise at each frequency. Paper II provides a more detailed derivation of the equations.

2.2.2 Results

In Paper II, the developed method was applied to a few simulated test structures on 128°-LiNbO$_3$ substrate. The metal thicknesses and the electrode widths of the single-electrode reflectors varied from one test structure to another. As an example of the extracted parameters, Fig. 2.7 shows the magnitudes of the reflection and transmission coefficients as a function of frequency. In this case the relative metal thickness was 2.5% and the electrode width was 0.8 μm. As reported in Paper II, the extracted parameter values agree well with those reported by Lehtonen *et al.* and Wang *et al.* The developed method offers a means of extracting frequency-dependent reflector parameters in a fast way without any specialized software or heavy calculation. The parameters can be extracted directly from simulated or measured test device S parameters.

3 SAW RFID Tag Designs

The main objective of this work has been to investigate whether SAW RFID tags can be a valid competitor for semiconductor-based tags. In pursuit of this goal, several ideas were tested. They involved tag geometries, encoding methods, loss reduction, and on-tag signal processing. Small size, large data capacity, reliability of identification, and minimal losses were the sought properties.

3.1 General Issues in Tag Design

In Papers III-V, SAW tags were designed and analyzed using FEM/BEM simulations. Device performance was further verified using experimental data obtained from network analyzer measurements. Similarly to the extraction of parameters discussed in Chapter 2, the tag analysis essentially relied on the simulated and experimental S parameters.

The SAW tag devices developed in this work use the same IDT for both generating and receiving surface acoustic waves. This makes them 1-port devices and their simulated as well as measured S matrices only contain one element, S_{11}. The tag design process has also necessitated the study of a few auxiliary test structures. These include, for example, a delay line comprising two identical IDTs facing each other. This structure has been used for estimating the losses due to transducers. The S_{21} parameter of this 2-port device includes the transduction and propagation losses, as well as eventual losses due to electrical mismatch. Simulations and experiments on two 2-port delay lines with different inter-IDT distances have been used for determining the free-surface SAW velocity on a given substrate.

Whenever referring to a surface acoustic wave in this work, a Rayleigh wave [132] is meant. It has its particle motion mainly in the sagittal plane (the plane containing the surface normal and the propagation direction) and its amplitude rapidly decreases with depth into the substrate. The substrate material for the developed SAW tag devices was chosen as $128°$-LiNbO$_3$. This cut has a low level of spurious responses [133], which is important for the distinguishing of coded responses from parasitic signals. Another interesting substrate would be the YZ-cut of LiNbO$_3$, which has the advantage of reduced diffraction effects. This is an attractive feature for SAW tags since they are long structures and a low level of losses is preferred.

3.1.1   Tag Responses

The simulated or measured S_{11} parameter gives the tag response to a delta pulse. However, in Papers III and IV, a more realistic idea of the response is desired. The studied tags are numerically excited using a sinusoidal pulse that has a Gaussian envelope, that is,

$$A(t) = e^{j\omega_0 t} e^{-a(t-T_{\text{pulse}}/2)^2}, \ \text{ for } \ 0 < t < T_{\text{pulse}}. \tag{3.1}$$

A pulse length of $T_{\text{pulse}} = 25$ ns is used and the pulse width is determined by $a = 1/(50 \ \text{ns}^2)$. The spectrum of the tag response is obtained through pointwise multiplication of the spectrum of the above defined interrogation signal with the simulated or measured S_{11} parameter.

As the time window T_W must be sufficiently large to accommodate even the reflections from the farthest reflectors, the chosen frequency step Δf must be sufficiently small, as suggested by Eq. (2.1). An adequate time resolution, for its part, is essential especially when the phases of response signals are studied. The time step Δt must be substantially shorter than the period of the surface acoustic wave. This imposes a lower limit, according to Eq. (2.2), on the frequency range for which S parameter data are needed. Since FEM/BEM simulation for tag structures is normally quite time-consuming, it is not reasonable to run very wide frequency bands, especially for frequencies where the acoustic response is known to be very small. It is better to use zero-padding or similar methods to artificially widen the frequency range and thus to improve the time resolution. In Papers III-V, zero-padding has been realized using excitation pulses defined for large frequency ranges.

One cycle of SAW is about 0.4 ns at 2.45 GHz and the time frame needed to fit in all the reflections is about 3 μs for the 14-reflector tags studied in Papers III and IV. In order to achieve a large enough time window and an adequate time resolution, data are needed for on the order of 10^5 frequency points. Performing such a full analysis would be a matter of weeks or even months of simulation time, depending on the computing capacity available. However, as the tag response is very weak outside the passband region, it is not reasonable to calculate exact data for these ranges. Instead, the zero-padding technique is used to artificially extend the frequency band (measured and simulated from 2250 MHz to 2650 MHz, in the case of Papers III and IV) down to 0 Hz and up to 40 GHz. This band yields a time resolution of 0.025 ns. With a frequency step of 0.25 MHz, a time window of 4 μs is obtained.
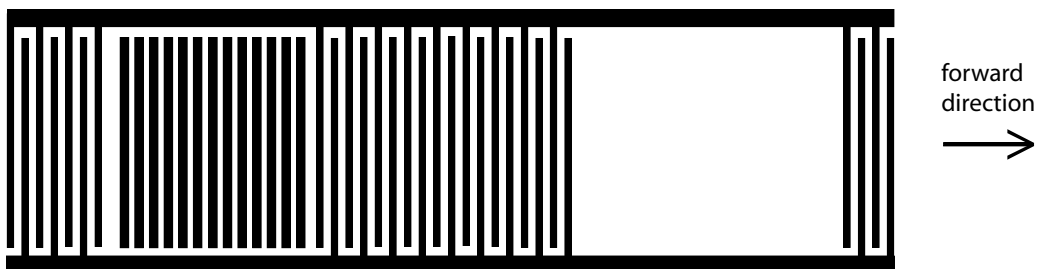
Figure 3.1: SPUDT geometry.

3.1.2 Transducer Design

As one of the goals for this work has been the reduction of losses in SAW tags, the bidirectionality loss inherent for standard IDTs had to be eliminated. This was accomplished by replacing the bidirectional IDT with a unidirectional transducer. In Papers III and IV, a SPUDT-type transducer was employed for generating and receiving surface acoustic waves. Inspired by the designs presented in [60], the SPUDT was designed to include a reflector section of open-circuited electrodes (14 electrodes) sandwiched by two standard transducer sections (7 electrodes on the side looking backward, 18 electrodes on the side looking forward), as shown in Fig. 3.1. For unidirectional operation, the reflector section was displaced by $\lambda/8$ from the position that would have been implied by the periodicity of the transducer section, as suggested in [48]. The forward generated waves thus interfere constructively with the backward generated but reflected waves. The backward generated waves interfere destructively with the forward generated but reflected waves. To obtain a rectangular passband of width B in the frequency domain, a negative time-sidelobe is needed at a distance of $t = 3/(2B)$ from the center of the SPUDT. This is achieved by adding a short transducer section, with electrode polarities flipped with respect to the periodicity implied by the main sections, on the side looking to the forward direction. The resistive losses are reduced by using two parallel signal paths, that is, by connecting two identical SPUDTs in parallel.

3.1.3 Reflector Array Design

As discussed in Sections 1.1.5 and 2.2, a SAW tag must include several (ten or more) code reflectors in order to achieve a reasonably large data capacity. This implies that the reflectors must have weak reflectivity and hence consist of only one or a few electrodes. In the tags reported in Papers III-V, the reflector strengths have been selected
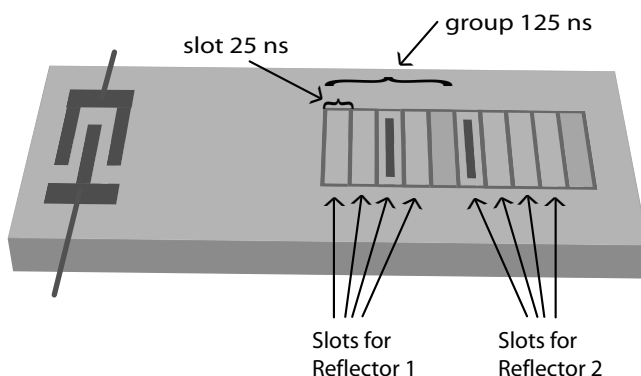
Figure 3.2: Principle of time position encoding. Schematic drawing.

so as to ensure uniform amplitudes of reflected pulses [63]. This is a way to improve the reading distance since the weakest signal actually determines the read range. In order to compensate for the propagation loss and losses due to reflections from preceding reflectors, code reflector reflectivity is gradually increased along the reflector array by increasing the number of electrodes in a reflector and by adjusting the metal ratio. The reflectivity of fundamental-mode ($p = \lambda/2$) open-circuited electrodes on $128°$-LiNbO$_3$ has been shown to increase with increasing metal ratio [118, 134].

For long structures, such as SAW RFID tags, diffraction effects can not be ignored. However, for the designs presented in this work, the device geometry (transducer aperture w compared to wavelength λ) is such that all the reflectors stay relatively well within the near-field region. The Fresnel limit x_c for the near-field zone is obtained from [135]

$$x_c = (1 + \gamma_a)\frac{w^2}{\lambda}, \tag{3.2}$$

where the anisotropy parameter γ_a has a value of -0.43 for $128°$-LiNbO$_3$ [136]. For the tags reported in Papers III and IV, $w = 155$ μm and $\lambda = 1.6$ μm, which gives $x_c = 8.6$ mm. The round-trip path lengths for the code reflections range from 4.7 mm to 10.9 mm. For an accurate compensation of diffraction effects, the straight open-circuited reflectors could be replaced with curved and segmented reflectors [61, 63]. The shape of these diffraction-compensated electrodes is matched to the shape of the incident SAW wavefront and their segmentation further prevents currents from flowing from one part of an electrode to another.

Figure 3.3: Mask image for a SAW tag having 14 reflectors.
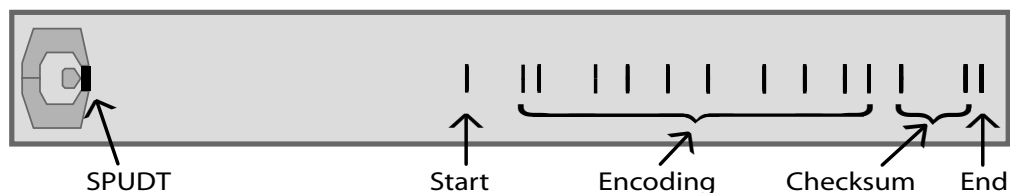
3.1.4 Encoding

The most straightforward way of encoding in SAW tags is the so-called time position encoding, which is based on the time delays of reflected pulses. This method was also used in Papers III-V, although combined with phase encoding in Paper IV. In this scheme, the total time delay is divided into slots of certain duration. To avoid intersymbol interference due to the time-overlapping of consecutive pulses, the slot width should roughly equal the time-width of the pulses. At 2.45 GHz, a band of $B_{\text{syst}} = 40$ MHz is typically used, and the corresponding slot width is thus $\Delta t_{\text{slot}} = 1/B_{\text{syst}} = 25$ ns. In Papers III-V, groups of 5 slots were formed. In each group, one of the first four slots was occupied by a reflector while the fifth one, the guard slot, was always left empty (see Fig. 3.2). Each reflector thus had four possible positions (equal to 2 bits of data) and the total number of different realizable codes was 4^n for a tag having n reflectors.

The tags presented in Papers III and IV have 14 reflectors, as shown in Fig. 3.3. However, only ten of them are used for encoding itself; the first and the last are used for calibration and are typically designed to have stronger responses than the others; and the two reflectors preceding the very last one are used for error control, for creating a checksum. Ten code reflectors will yield about 10^6 distinct codes. When all the reflectors are placed in-line in one acoustic path, the chip space required by these 10 reflectors is about 2.5 mm.

When decoding, the time positions of code reflections are easily and reliably attributed to a code sequence by first locating the calibration reflections, then dividing the time span in-between into an appropriate number of slots and groups, and finally determining for each group the slot that corresponds to the local maximum of the response signal.

3.2 Z-Path SAW RFID Tag

As a SAW identification tag must provide a sufficient time delay in order to separate environmental echoes from the coded signal, one of its essential functions is to act
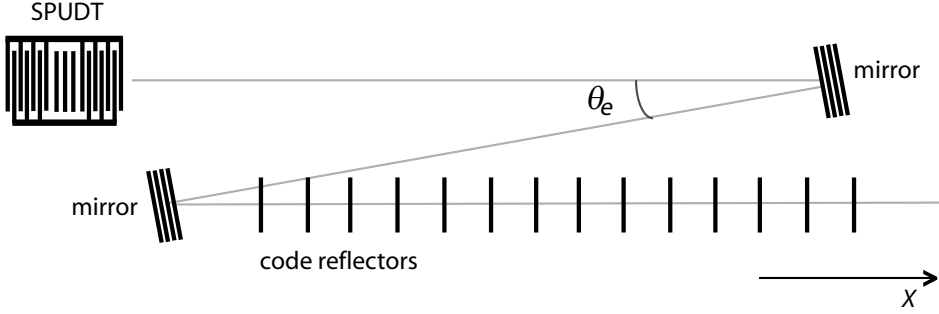
Figure 3.4: Schematic drawing of the Z-path geometry. The SAW beam (energy) is reflected through an angle θ_e at the inclined reflectors.

as a delay line. Time delay is implemented by leaving a region of free surface on the substrate between the transducer and the encoding elements. An adequate initial delay is normally about 1 μs, which roughly corresponds to a propagation distance of 4 mm on 128°-LiNbO$_3$. For a tag using reflectors for encoding, the needed length of free surface thus is 2 mm.

Inline tag geometries often result in rather long and narrow structures. The tag length can be reduced by folding the propagation path of the surface wave. In Paper III, a Z-path geometry, previously used for miniaturization of SAW filters [137], has been employed. It involves using two weakly inclined reflectors, as sketched in Fig. 3.4, and allows the use of the same space in the crystal X-direction for both the initial delay and the code reflectors. No space is needed for the initial delay alone. However, the anisotropy of the substrate material has to be taken into account in the design of the Z-path geometry.

3.2.1 Design

Due to the anisotropy of the substrate material, the phase velocity v of the surface acoustic wave is a function of the propagation direction θ. This dependence is often illustrated using a slowness curve, which is a polar plot of the phase slowness s of the surface wave, defined as $s(\theta) = 1/v(\theta)$. The slowness curve for 128°-LiNbO$_3$ is presented in Fig. 3.5a with $\theta = 0°$ corresponding to the X-direction.

The reflection of a SAW from an inclined reflector can be examined in terms of the wave vectors $\vec{k}_i$, $\vec{k}_r$, and $\vec{k}_G$, as shown in Figs 3.5b and 3.5c. The vectors $\vec{k}_i$ and $\vec{k}_r$ represent the incident and reflected SAWs, respectively, and $\vec{k}_G$ is associated with the inclined reflector, treated here as a coupler between the incident and reflected waves.
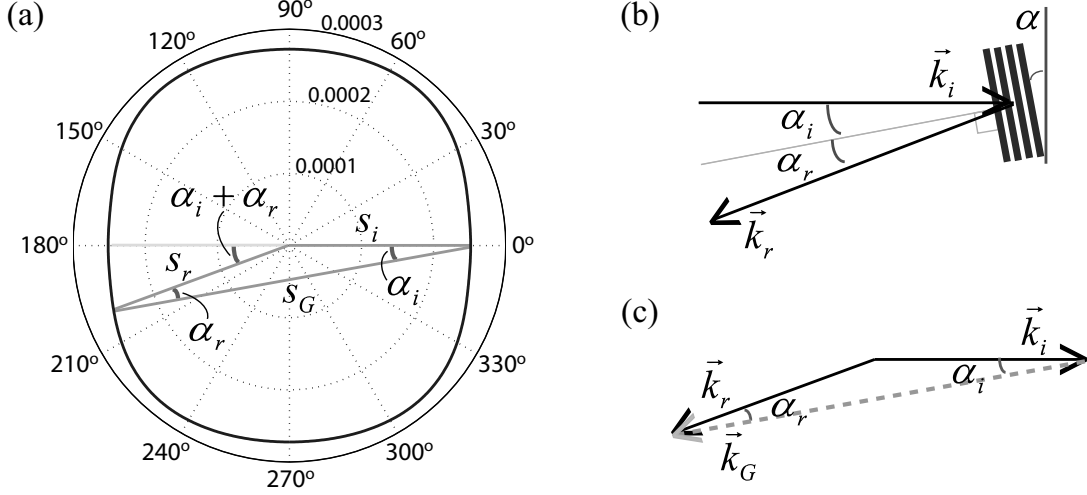
Figure 3.5: (a) Slowness curve for the free surface of 128°-LiNbO$_3$ [139]. Values of slowness are in seconds/meter. (b) Wave reflection at an inclined reflector. (c) Wave vector diagram for a reflection at an inclined reflector.

The grating wave vector $\vec{k}_G$ is normal to the reflector electrodes and its magnitude equals $2\pi/p_G$, where p_G is the electrode pitch of the inclined reflector. As shown in Fig. 3.5c, the wave vectors $\vec{k}_i$, $\vec{k}_r$, and $\vec{k}_G$ are related by the equation $\vec{k}_i + \vec{k}_G = \vec{k}_r$ [98, 138].

As a wave vector $\vec{k}$ can be written as $\vec{k} = 2\pi f \vec{s}$, where f is the frequency of the wave, a scaled version of the triangle of Fig. 3.5c can be superimposed on the slowness curve. The sides of the scaled triangle of Fig. 3.5a are the magnitudes s_i and s_r of slowness for the incident and reflected waves, and the magnitude of the slowness $\vec{s}_G$ corresponding to $\vec{k}_G$. The values of s_i and s_r are given by the slowness chart while s_G can be written as $s_G = 1/(p_G f)$. The angles of incidence α_i and reflection α_r (which are not equal due to the different velocities of the incident and reflected waves) as well as the reflector pitch p_G can be determined using this triangle once $\alpha_i + \alpha_r$ is fixed. The angle $\alpha_i + \alpha_r$ gives the direction of the reflected wave vector $\vec{k}_r$ with respect to the (negative) X-direction.

However, substrate anisotropy also implies that the direction of energy flow θ_e (see Fig. 3.4) deviates from the direction of the wave vector, θ. The difference between these two angles is called the power flow angle and can be obtained as [140]

$$\theta - \theta_e = \arctan\left(\frac{1}{v}\frac{dv}{d\theta}\right), \tag{3.3}$$
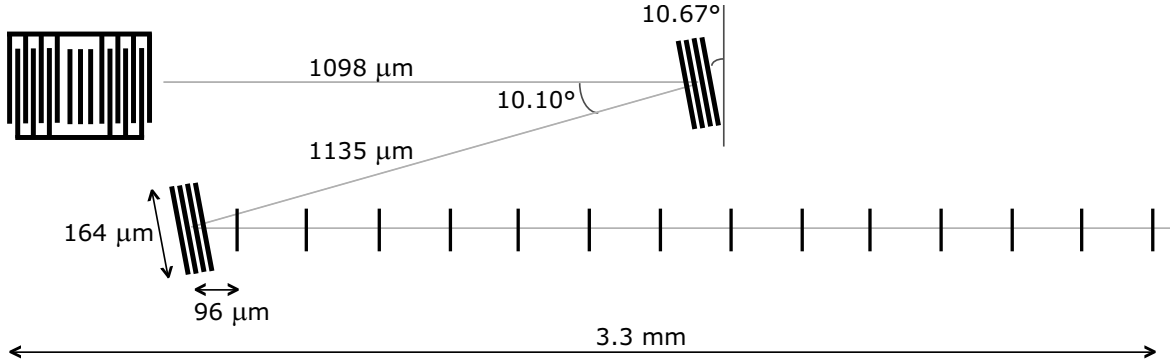
Figure 3.6: Z-path design.

where θ and θ_e are in radians.

Calculating the Z-path geometry actually reduces to fixing the positions of the inclined mirrors and then finding their correct angle of inclination α. The inclination angle α, in fact, equals α_i, as can be seen from Fig. 3.5b. By fixing the mirror positions, one also fixes the direction of energy flow θ_e. With θ_e fixed, the corresponding wave vector direction can be determined using Eq. (3.3). This propagation direction corresponds to $\alpha_i + \alpha_r$. The electrode pitch p_G of the inclined reflector as well as the angles α_i and α_r can be determined from Fig. 3.5a through successive application of the cosine and sine theorems.

3.2.2   Results

The design of the Z-path SAW tag presented in Paper III is shown in Fig. 3.6. The device length is about 2 mm shorter than for an equivalent inline design. Figure 3.7 shows the measured response of this 2.45-GHz SAW tag to the interrogation signal described by Eq. (3.1). As can be seen, the uniformity of peaks is excellent and the level of losses is good with the code peaks roughly at -55 dB. The loss level can still be improved through optimization of the inclined reflectors.

3.3   Phase-Encoded SAW RFID Tag

One of the objectives of this work was to enhance the data capacity of SAW RFID tags. When employing the time position encoding method described above, only the time delay information of the reflected pulses is used and each code reflector has 4 possible positions, corresponding to 2 bits of data. However, the data capacity can be significantly enhanced, if also the phase information of the response signals is used. An inline
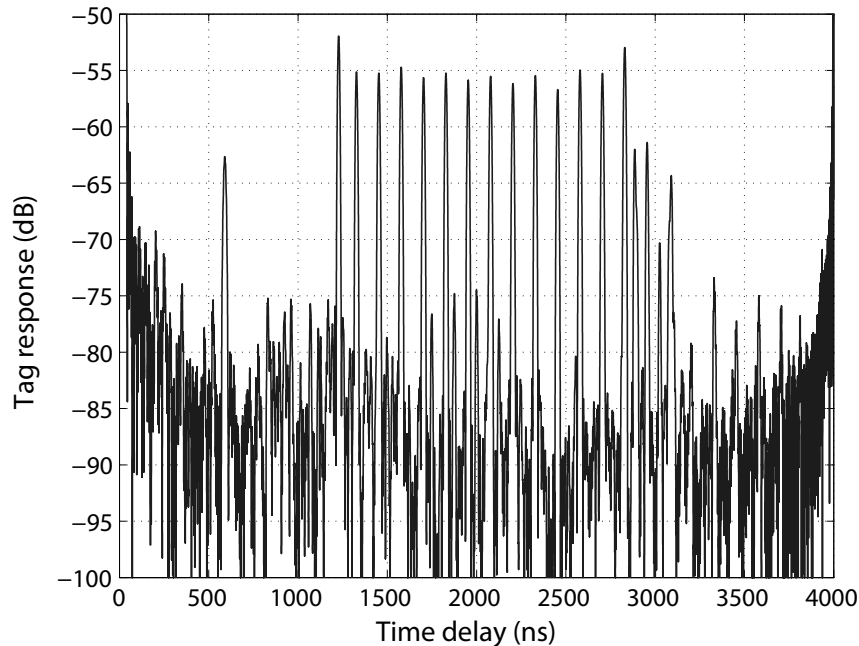
Figure 3.7: Response of the Z-path SAW tag of Fig. 3.6. Experimental data.

SAW tag that combines time position encoding with phase encoding was designed and implemented in Paper IV. For this tag, time position encoding is used as described in Section 3.1.4. In addition, a phase shift of 0°, -90°, -180°, or -270° is introduced by shifting the reflector positions by multiples of $\lambda/8$, as shown in Fig. 3.8. This yields an additional 2 bits of data per reflector.

3.3.1 Decoding

In order to extract the phase information of the reflected pulses, the time response is divided by a reference signal of the form $e^{j\omega_0 t}$, where ω_0 refers to the center frequency of the interrogation pulse. In this way, the phase of the response signal is compared with that of the reference signal, and the reflections from the code reflectors are expected to be represented by segments of constant phase.

In the design, it was assumed that the SAW velocity on 128°-LiNbO$_3$ is 3978.48 m/s, and the center frequency 2441.75 MHz of the frequency band allocated for industrial, scientific, and medical applications (ISM) was used. This corresponds to a wavelength of 1.629 μm, which was used to determine the positions of the reflectors and hence to yield the desired phases for the reflected signals. However, both the velocity assumed
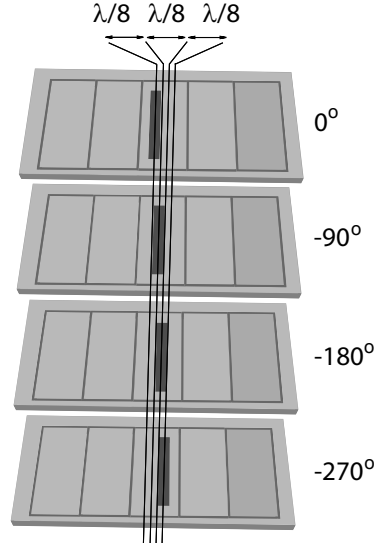
Figure 3.8: Principle of phase encoding. Proportions are not to scale.

in the FEM/BEM simulator and the actual real-world velocity are different from that assumed in the design. Although small, these differences are sufficient to bring about significant phase changes. Also, while the design was made for a single frequency point, the actual device must be decodable for a full range of frequencies within the operating band. The observed wavelength is thus usually not equal to the wavelength assumed in the design. The distances between the SPUDT and the reflectors also vary with temperature changes. In order to compensate for these effects, all extracted phase data must be corrected accordingly using a linear calibration function (linear dependency on time delay).

In order to determine the slope of the linear correction, the number of wavelengths corresponding to a short distance on chip is compared for design and experiment. The experimental value is obtained from

$$N_\lambda = f_c \Delta\tau, \tag{3.4}$$

where f_c is the center frequency of the interrogation pulse and $\Delta\tau$ is the experimentally observed time delay corresponding to the short distance. In principle, accurate analysis requires two reflectors (preferably the first two in the array) to lie sufficiently close to each other. In particular, their separation must be such that the difference between the designed and experimental total phases corresponding to this distance stays within $\pm 2\pi$. If this is the case, phase ambiguity is avoided and the slope of the linear phase correction can be obtained as the ratio of the difference between the experimental and
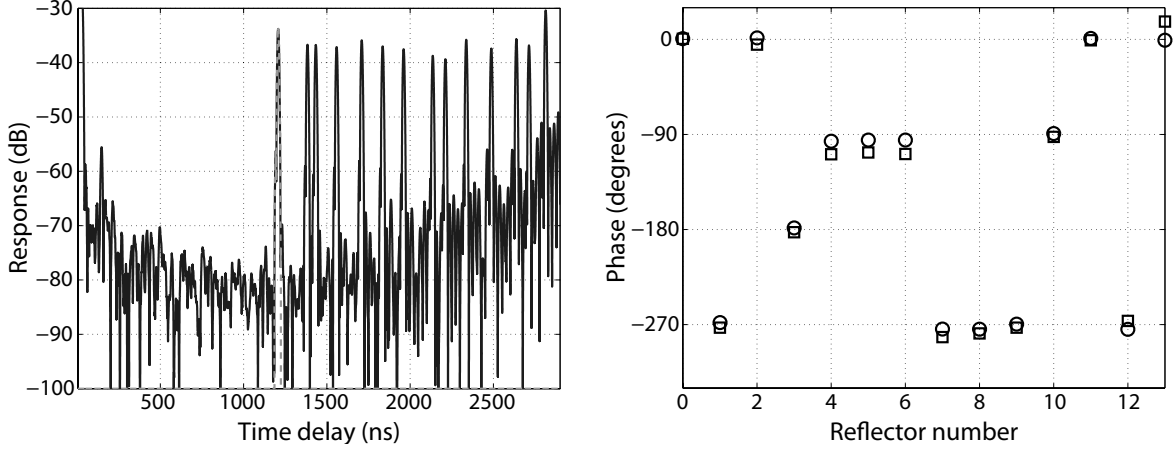
Figure 3.9: *Left:* Experimental response of an inline tag sample. The dashed line indicates the time-gating of the first reflection. *Right:* Simulated (circles) and measured (squares) phases for a phase-encoded tag after phase corrections.

designed phases with the time delay corresponding to the short distance in question. As the tag design presented in Paper IV does not include such short delays, the difference of two similar delays has been used in order to obtain a sufficiently short delay. Resembling techniques were proposed in [39] and [141] for temperature sensors.

3.3.2 Results

Figure 3.9 (left) presents a typical experimental response for an inline time-position and phase-encoded tag sample. This result can be used to extract the time-position-based code in the straightforward manner described in Section 3.1.4. The loss level, that is, the ratio of the amplitudes of the code reflections to the amplitude of the interrogation signal, is about -38 dB. For comparison, an insertion loss of -53 dB was achieved for the weakest code reflections in [63]. The difference is due to the fact that in this work, a unidirectional transducer was used and the structure of the reflector array was carefully optimized.

Extraction of phase data presented an additional challenge as the procedure proposed in Section 3.3.1 did not produce flat line segments for the phases of the reflected signals. This anomaly was found to be due to phase distortion caused by the SPUDT. Based on delay line simulations, the phase error was estimated to be 5° to 10° depending on frequency. The distortion was eliminated and flat line segments obtained by dividing the spectrum of the total tag response by the spectrum of the first reflection

(indicated by a dashed line in Fig. 3.9). This procedure is based on the fact that each reflective echo includes a contribution from the SPUDT, from free-surface propagation, from the reflector at which the reflection has occurred, and from all the reflectors preceding that reflector. When dividing the spectrum of the total tag response by the spectrum of the first reflection, the transducer contribution (along with the round-trip propagation between the IDT and the first reflector, and the reflection from the first reflector) is eliminated from each reflection.

Figure 3.9 (right) presents the phase data (simulated and experimental) for a phase-encoded tag sample. After the phase corrections described in 3.3.1 and the elimination of the SPUDT contribution, the phase-based code can be identified without any ambiguity.

3.4   Ultra-Wideband SAW RFID Tags

The feasibility of UWB SAW RFID tags was studied in Paper V. As the main goals in the development of this tag were the reduction of tag size and the reinforcement of resistance to environmental echoes, a natural choice was to use chirp signals and matched-filter operation.

3.4.1   Principles of Signal Processing Within the UWB SAW Tag

The analysis of a chirped device involves processing of linear frequency modulated (LFM) signals, which can be written as [142]

$$s(t) = a(t) \cos \left[\theta(t) \right]. \tag{3.5}$$

A standard chirp signal has a flat unit amplitude, in which case $a(t)$ is set to unity for $0 < t < T_{\text{chirp}}$ and to zero otherwise. T_{chirp} denotes the length of the chirp pulse. The phase $\theta(t)$ is given by the quadratic function

$$\theta(t) = \pi\mu \left(t - \frac{T_{\text{chirp}}}{2} \right)^2 + 2\pi f_c \left(t - \frac{T_{\text{chirp}}}{2} \right) + \phi_0, \tag{3.6}$$

where $\mu = \pm B/T_{\text{chirp}}$ is the chirp rate, B is the used frequency band, f_c is the center frequency, and ϕ_0 is a constant. Waveforms with $\mu > 0$ are called up-chirps and those with $\mu < 0$ are called down-chirps. In this Section, these signals are referred to by $s_{\text{up}}(t)$ and $s_{\text{down}}(t)$, respectively.

The principle of signal processing during tag interrogation is schematically illustrated in Fig. 3.10 for a case where the interrogation signal is an up-chirp pulse. If the impulse response of the transducer on the tag is the time-reverse of the interrogation
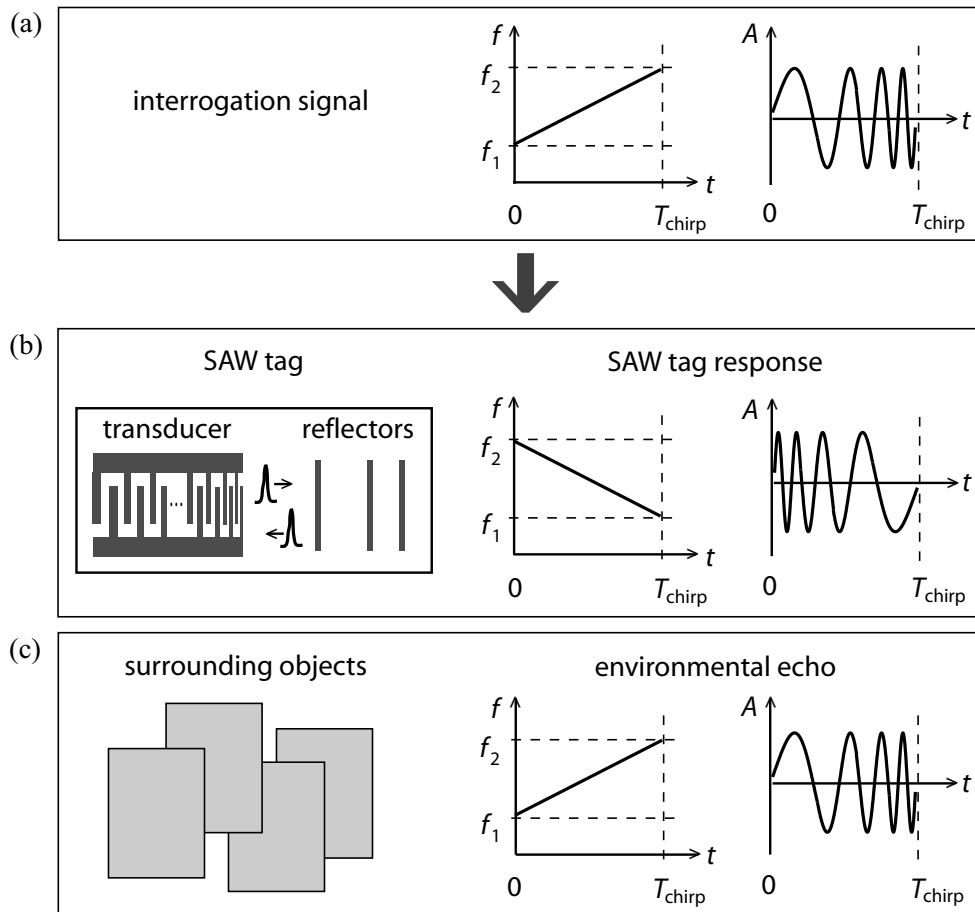
Figure 3.10: Interrogation process. (a) An up-chirp LFM signal is used for interrogation. (b) The signal is compressed by the chirp transducer, reflected by the code reflectors, and expanded by the transducer. The output has a dispersion opposite to that of the interrogation signal. (c) Reflections from surrounding objects have the same dispersion as the interrogation signal.

signal, then the SAW pulse propagating on the surface of the substrate will be a narrow correlation peak. When this compressed pulse returns to the transducer and is retransmitted by the tag antenna, the output signal will essentially be the time-reverse of the interrogation signal. However, the reflections of the interrogation signal from surrounding objects, that is, the environmental echoes, will have the same waveform as the interrogation pulse. When the tag responses together with the environmental echoes are detected at the reader, matched-filtering is performed such that only the tag response will be compressed. The use of chirp signals and matched-filter operation thus offers a means for distinguishing the useful signal from parasitic reflections.

3.4.2 Design

As sketched in Fig. 3.10b, the proposed UWB SAW tag consists of a chirp transducer and an array of narrow code reflectors. The positions of the transducer electrodes must be chosen in accordance with the anticipated waveform to be launched [143]. As the impulse response of the transducer must now be linearly frequency-modulated, the electrode pitch should gradually decrease or increase depending on the type of chirp desired. The electrode positions can be determined by finding the points at which $s(t) = 1$ or $s(t) = $ -1. It can readily be shown that the total number of cycles in $s(t)$ is $f_c T_{\text{chirp}}$. Assuming $\theta(0) = 0$, the time positions t_n of the electrodes can be solved from the equation $\theta(t_n) = n\pi$, where $n = 0,1,2,\ldots,2f_c T_{\text{chirp}}$. This yields

$$t_n = -\frac{f_1}{\mu} \pm \sqrt{\left(\frac{f_1}{\mu}\right)^2 + \frac{n}{\mu}}, \tag{3.7}$$

where the plus-sign is used for $\mu > 0$ and the minus-sign for $\mu < 0$. In Eq. (3.7), $f_1 = f_c \mp B/2$ is the starting frequency of the chirp (the minus-sign is for $\mu > 0$ and vice versa). The physical positions x_n of the electrodes on the substrate surface are given by $x_n = v t_n$, where v is the SAW velocity on the substrate.

As the tag response and the environmental echoes are distinguished from each other by using matched-filter techniques, the initial delay can be drastically shortened. In experiments, 150 ns was used instead of the 1 μs needed in ordinary SAW tags. In a UWB tag operating within a frequency band of 500 MHz, the code reflectors can be placed in slots as narrow as 2 ns, which corresponds to the width of the compressed pulse propagating on the substrate surface ($\Delta t_{\text{slot}} = 1/B_{\text{syst}} = 1/500\,\text{MHz} = 2\,\text{ns}$). The reflectors can thus be placed closer to each other than in conventional SAW tags (operating at 2.45 GHz with a band of 40 MHz), where the slots typically are 25 ns wide. The shortening of the initial delay and the denser array of code reflectors result in a very compact tag geometry.

3.4.3 Analysis

The operation of the designed UWB SAW tag was analyzed based on the simulated and measured S_{11} parameter. The studied tag had a transducer with high-frequency sections closest to the code reflectors and was interrogated using an up-chirp signal. In order to decrease the level of the time-sidelobes of the correlation peak, the flat-envelope interrogation signal introduced in Eq. (3.5) was weighted using a cosine window as

$$s_{\text{up,w}}(t) = a(t) \cos\left[\theta(t)\right] \cos\left(\frac{\pi t}{T_{\text{chirp}}} - \frac{\pi}{2}\right). \tag{3.8}$$

The spectrum of the tag output $G(f)$ was obtained by multiplying the spectrum of the interrogation signal $S_{\text{up,w}}(f)$ by the simulated or experimental S_{11} parameter. This can be written as

$$G(f) = S_{\text{up,w}}(f)S_{11}(f), \tag{3.9}$$

where $S_{\text{up,w}}(f)$ is the Fourier transform of $s_{\text{up,w}}(t)$. The parameter $S_{11}(f)$ can be considered the frequency response of the tag device. The tag response $G(f)$, or its inverse Fourier transform $g(t)$, is compressed by using a matched filter whose impulse response is of the form $s_{\text{up}}(t)$, that is, essentially the time-reverse of $g(t)$. The spectrum of the compressed tag response $C(f)$ is thus obtained from

$$C(f) = G(f)S_{\text{up}}(f), \tag{3.10}$$

and the time-domain response $c(t)$ can finally be calculated as the inverse Fourier transform of $C(f)$.

The compressed tag response can also be obtained by interrogating the tag with an up-chirp signal of duration $2T_{\text{chirp}}$ and band B, that is, by replacing μ with $\mu/2$. The output will then be a train of compressed pulses.

3.4.4 Results

Paper V presents a UWB SAW tag design that includes a chirp transducer and 10 code reflectors. The device is shown in Fig. 3.11 and its chirp transducer in Fig. 3.12. The chirp IDT operates at a center frequency of $f_c = 1$ GHz and has a band of $B = 500$ MHz. Such a low center frequency was chosen in order to keep the simulation time reasonable. (For higher frequencies, a significantly larger number of transducer electrodes is needed to produce a chirp of certain duration. The simulation time increases rapidly with the increase of the number of electrodes.) The designed transducer consists of 100 pairs of electrodes and has a length of about 400 μm. The chirp duration is $T_{\text{chirp}} = 100$ ns.

Figure 3.11: Photograph (taken through a microscope) of the fabricated UWB SAW tag device. The length of the structure is 1.1 mm.
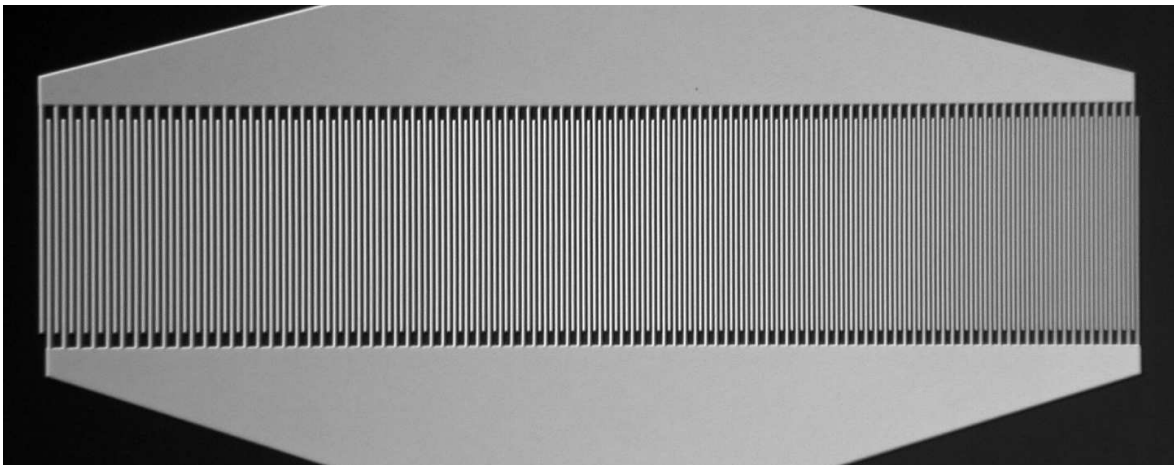

Figure 3.12: Photograph of the chirp transducer of the UWB SAW tag shown in Fig. 3.11. The low-frequency sections are on the left and the high-frequency sections on the right. The transducer length is 400 μm and aperture 75 μm.
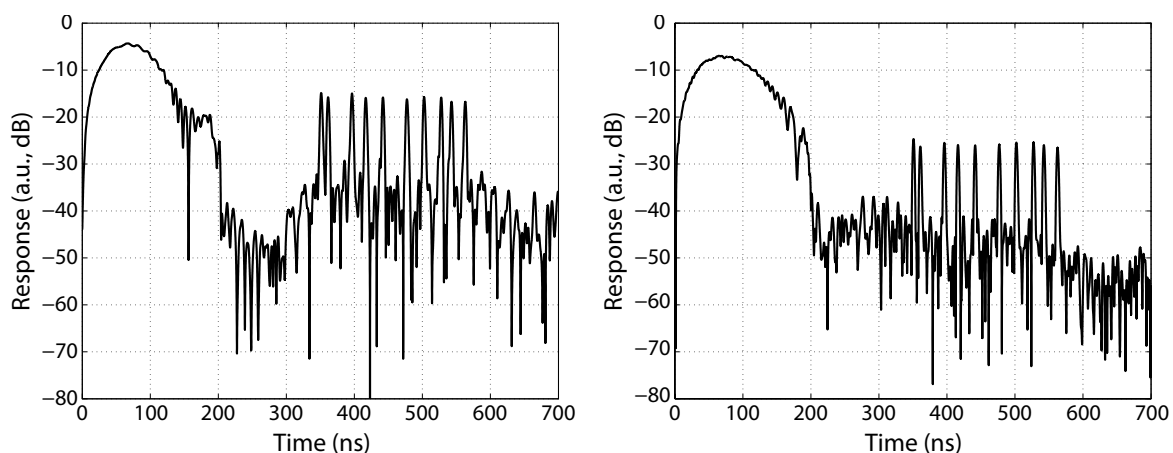
Figure 3.13: Compressed response of a UWB SAW tag device having 10 code reflectors. *Left:* Simulated. *Right:* Experimental.

For this tag, encoding is based on groups of 5 slots with a slot width of 5 ns. The initial delay is reduced to 150 ns and the length of the entire structure is only 1.1 mm.

The device was simulated using FEM/BEM software and fabricated on 128°-LiNbO$_3$ using electron beam lithography and liftoff process. Figure 3.13 shows the simulated (left) and experimental tag responses (right). In both cases, the compressed response is obtained by applying an ideal chirp signal with band $B = 500$ MHz and duration $2T_{\text{chirp}} = 200$ ns directly to the simulated or measured S_{11} data. The level of the compressed peaks is comparable between the two cases. Both responses illustrate the fact that the total delay is significantly shorter than with ordinary SAW tags.

The UWB SAW tag is feasible. It will be small in size and it will have a reasonably large data capacity. Estimation of reading range, in Paper V, showed that it can be interrogated with readers radiating a very low power and still achieve reading ranges sufficient for many applications. The FCC regulation [73–75] allows a reader power of -41.3 dBm/MHz for frequencies higher than 1.99 GHz. For an operating bandwidth of $B = 500$ MHz (from 2.0 GHz to 2.5 GHz), this corresponds to a total radiated power of 37 μW and an estimated reading range of about 2.4 m. The achievable reading range evidently depends on the integration time and other reader characteristics.

4   Discussion and Conclusion

In this thesis, new variants of surface acoustic wave RFID tags were designed and analyzed using simulations and experiments. In Papers I and II, the research done on the extraction of reflector parameters was presented. The reflectivity and SAW attenuation of narrow metal electrodes were determined, and a new method for extracting the reflection, transmission, and scattering parameters of short metal reflectors was developed. Papers III-V focused on the design of SAW RFID tags. Novel tag designs were presented, including a Z-path SAW RFID tag having a reduced size, and a tag combining time position and phase encoding and thus having an enhanced data capacity. The feasibility of ultra-wideband SAW RFID tags was investigated and a UWB SAW tag with a compact size and strong resistance to environmental echoes was designed and implemented.

4.1   Extraction of Reflector Parameters

The first part of the thesis discussed the extraction of the central SAW reflector parameters. An accurate knowledge of the reflection, transmission, and scattering parameters is essential when SAW RFID tags or DDL devices are developed.

Paper I studied the applicability of narrow electrodes to the development of dispersive delay lines. Such narrow metal strips are needed in SAW tags as well in order to achieve a sufficiently weak reflectivity. However, only fragmentary data on the reflectivity of narrow metal electrodes was available in previous publications [112–116]. In Paper I, it was estimated that a controllable reflectivity of $r < 0.3\%$ per electrode is required in order to design inline DDLs with reasonable parameters. It was demonstrated, using simulations and experiments, that narrow open-circuited aluminum electrodes are perfectly suitable for this application. Reflectivities of desired magnitude can easily be achieved and they can be controlled by varying the electrode width. Today, standard optical lithography can produce sufficiently narrow linewidths to render metal strips a valid alternative to grooves, previously used in RACs.

In Paper II, a new method for determining the reflection, transmission, and scattering parameters for short metal reflectors was developed. An accurate knowledge of these parameters is essential in tag design. Previous methods [118–121] either did not consider the frequency-dependence of the parameters or involved the use of specialized software. The new method uses the FEM/BEM-computed S parameters of a SAW tag device to analytically extract the reflection and transmission coefficients (absolute values and phase angles) and the energy scattered into bulk as a function of frequency. Assuming the S parameters available, this is a simple and very fast way to characterize

short metal reflectors without heavy calculation or specialized software. Although only used for simulated data in Paper II, the developed method has the advantage of being applicable to measured data as well.

4.2 SAW RFID Tag Designs

The main focus of this thesis is on the design of novel SAW RFID tags. In Paper III, a reduced tag size was achieved by employing a Z-path acoustic channel. In Paper IV, data capacity was enhanced by combining time position encoding with phase encoding. And finally, in Paper V, the feasibility of ultra-wideband SAW tags that meet the FCC rules [73–75] for UWB applications was validated.

4.2.1 Z-Path SAW Tag

Previously reported SAW tags used a bidirectional IDT and an inline arrangement of code reflectors [34,39]. This resulted in a relatively large chip size of about 1 x 10 mm^2. In Paper III, a design and experimental results for an improved SAW tag were presented. Tag size and losses were reduced by replacing the bidirectional IDT with a unidirectional IDT. A further reduction of device size was achieved by adopting a Z-path geometry. Two inclined reflectors were used to fold the propagation path. The advantage of this configuration is that the same space in the X-direction is used for both the initial delay and the code reflectors. No space is needed for the initial delay alone. This means that the chip length is finally determined only by the space required by the code reflectors. The Z-path geometry allows for a reduction of tag length by about 2 mm as compared to an equivalent single-track configuration using a unidirectional IDT with the code reflectors placed in-line. The proposed configuration is especially advantageous for tags having a relatively long initial delay compared to the space required by the code reflectors. For such devices, a chip size of less than 1 x 2 mm^2 (at 2.45 GHz) is realizable. Another advantage of the Z-path configuration is that the direction of the twice reflected wave always remains parallel to the initial direction. This makes the device operation practically insensitive to the temperature variations of size and wave velocities. A U-path geometry [38], for example, would not have this advantage.

4.2.2 Phase-Encoded SAW Tag

In Paper IV, it was shown that the data capacity of SAW RFID tags can be significantly enhanced by combining the time delay information of reflective echoes with phase data.

In the presented tags, each echo has four possible time positions and four possible phases. With ten reflectors used for encoding, this results in 10^{12} unique codes (40 bits), which is a significant improvement compared to the 10^6 distinct codes (20 bits) that may be realized when using time delays alone. In addition to the enhanced data capacity, a low loss level of -38 dB was achieved for the reflective echoes.

Extracting and interpreting the phase information of reflected signals demands precise knowledge of reflector parameters, even in the case of tags having a relatively small number of code reflectors as those presented in Paper IV. Reflection and transmission phase shifts must be known accurately. For unambiguous phase calibration, the separation of the first two reflectors must be short and fixed. Other calibration procedures, such as using a reference tag with known phase information, can also be employed for robust algorithms of reading phase-encoded SAW tags.

In Paper IV, it was found that the SPUDT used for launching and receiving surface acoustic waves causes a phase distortion of a few degrees. With only four different phases used for encoding, the compensation of this distortion is not necessary. However, it will become critical if the phase step for encoding is to be reduced from the $90°$ used in the present work. Then, a reliable extraction of phase-based codes requires eliminating the SPUDT phase distortion.

Phase encoding methods are currently intensively investigated [144]. The uncertainty of determining the signal phase depends on the signal-to-noise ratio. When phase encoding is used, the number of codes per certain chip length increases but a higher signal-to-noise ratio is required, decreasing the reading range of the tag.

4.2.3   Ultra-Wideband SAW RFID Tags

The feasibility of ultra-wideband SAW RFID tags was studied in Paper V. The UWB technology gives SAW tags significant advantages. First of all, with wider available bands, a certain BT (the product that determines the information capacity of the tag) can be obtained with a shorter coding time T. For example, with $B = 500$ MHz, a BT of 200 only requires a coding time of 400 ns instead of the 2 μs typical for 2.45-GHz SAW tags. With such a coding time, the total length of a SAW chip can be shorter than 1 mm. In Paper V, it was experimentally demonstrated that a UWB SAW tag with 10^6 different codes can have a chip size of about 0.5 x 1 mm^2.

Another attractive possibility related to the use of the UWB technology is performing signal processing within a SAW tag. Using a chirp transducer in the tag allows for a matched-filter processing of the tag response. In this case, the dispersion of the interrogation signal is modified within the tag. The tag response thus differs from the reflections of the interrogation signal from other objects. This makes the system more

resistant to echoes from the surroundings. Typically, an initial delay of 1 μs is needed in ordinary SAW tags for the decay of environmental echoes. With UWB tags, this delay can be significantly shorter.

A shorter total delay also implies lower propagation losses. A propagation time of 400 ns corresponds to only about -3 dB of propagation loss on 128°-LiNbO$_3$. In ordinary SAW tags, the total delay is about 2 μs to 4 μs, and propagation loss correspondingly on the order of -20 dB. UWB SAW tags may then have a reduced total loss despite the increased loss in the dispersive transducer.

Finally, the reader power may be very low for UWB SAW tags. In the estimations formulated in Paper V, the total power radiated by a reader is lower than 40 μW. This is undeniably an attractive level, although the reading range is expected to be limited to about 2 m to 5 m depending on the integration time and other reader characteristics. For short reading distances, the interrogation signal will be radiated for about 1 ms per one reading. This puts the average power at the nanowatt level, assuming reading of one tag sufficient for many applications. A reduction in the reader power also implies a reduction of human exposure to electromagnetic radiation. This should have a positive impact on the general public's attitude to new wireless services.

4.3   Conclusion

For RFID tags, the two most important issues are the price, which is related to the chip size, and the power radiated by the reader. In this thesis, it was shown that SAW-based tags present a viable alternative to semiconductor tags. The competitiveness of SAW RFID as an automatic identification method was substantiated by experimental evidence. Novel SAW RFID tag designs that combine a small size and a data capacity sufficiently large for many applications were presented. In particular, taking SAW tags to the ultra-wide bands holds great promises such as a drastic reduction of device size, a stronger resistance to environmental echoes, and a very low reader power.

References

[1] M. Cardullo and W. L. Parks, "Transponder apparatus and system", 1973, U. S. Patent no. 3713148.

[2] S. Shepard, *RFID Radio Frequency Identification.* New York: McGraw-Hill, 2005.

[3] H. Hollerith, "Apparatus for compiling statistics", 1889, U. S. Patent no. 395783.

[4] N. J. Woodland and B. Silver, "Classifying apparatus and method", 1949, U. S. Patent no. 2612994.

[5] GS1, "GS1 general specifications", version 8.0, issue 2, 2008, http://www.gs1uk.org.

[6] W. Buff, J. Ehrenpfordt, S. Klett, M. Rusko, and M. Goroll, "On-chip correlation - a new approach to narrow band SAW identification tags", in *Proc. 1998 IEEE Ultrasonics Symposium*, pp. 385–388 (1998).

[7] C. S. Hartmann, P. Hartmann, P. Brown, J. Bellamy, L. Claiborne, and W. Bonner, "Anti-collision methods for Global SAW RFID tag systems", in *Proc. 2004 IEEE Ultrasonics Symposium*, vol. 2, pp. 805-808 (2004).

[8] P. J. Edmonson and C. K. Campbell, "Encoded SAW RFID tags and sensors for multi-user detection using IDT finger phase modulation", 2004, U. S. Patent no. 6827281.

[9] C. S. Hartmann and J. C. Bellamy, "Transfer function system for determining an identifier on a surface acoustic wave identification tag and method of operating the same", 2005, U. S. Patent no. 6958696.

[10] P. Brown, P. Hartmann, A. Schellhase, A. Powers, T. Brown, C. Hartmann, and D. Gaines, "Asset tracking on the International Space Station using Global SAW tag RFID technology", in *Proc. 2007 IEEE Ultrasonics Symposium*, pp. 72–75 (2007).

[11] B. Lee and H. Kim, "Design and implementation of a secure IBS platform using RFID and sensor network", in *Proc. 2006 IEEE Tenth International Symposium on Consumer Electronics*, pp. 1–4 (2006).

[12] F. Thiesse, E. Fleisch, and M. Dierkes, "LotTrack: RFID-based process control in the semiconductor industry", *IEEE Pervasive Computing* **5**, pp. 47–53 (2006).

[13] F. Liu and Z. Miao, "The application of RFID technology in production control in the discrete manufacturing industry", in *Proc. 2006 IEEE International Conference on Video and Signal Based Surveillance*, pp. 68–73 (2006).

[14] X. Jiang and X. Wang, "Study on logistic information acquisition technology in steelmaking practice based on RFID", in *Proc. 7th World Congress on Intelligent Control and Automation*, pp. 7946–7950 (2008).

[15] B. C. Hardgrave, M. Waller, and R. Miller, "RFID's impact on out of stocks: a sales velocity analysis", 2006, RFID Research Center, Information Technology Research Institute, Sam M. Walton College of Business, University of Arkansas.

[16] M. D. Mills-Harris, A. Soylemezoglu, and C. Saygin, "RFID data-based inventory management of time-sensitive materials", in *Proc. 31st Annual Conference of IEEE Industrial Electronics Society*, pp. 2302–2307 (2005).

[17] G. Liu, W. Yu, and Y. Liu, "Resource management with RFID technology in automatic warehouse system", in *Proc. 2006 IEEE/RSJ International Conference on Intelligent Robots and Systems*, pp. 3706–3711 (2006).

[18] T. Hoven, "The Trondheim toll ring. The political process and the technical solutions." in *Proc. 6th International Conference on Road Traffic Monitoring and Control*, pp. 24–27 (1992).

[19] L. Reindl, G. Scholl, T. Ostertag, H. Scherr, U. Wolff, and F. Schmidt, "Theory and application of passive SAW radio transponders as sensors", *IEEE Trans. Ultrason. Ferroelectr. Freq. Control* **45**, pp. 1281–1292 (1998).

[20] R. Weinstein, "RFID: a technical overview and its application to the enterprise", *IT Professional* **7**, pp. 27–33 (2005).

[21] B. Nath, F. Reynolds, and R. Want, "RFID technology and applications", *IEEE Pervasive Computing* **5**, pp. 22–24 (2006).

[22] X. Zhang, S. Yue, and W. Wang, "The review of RFID applications in global postal and courier services", *The Journal of China Universities of Posts and Telecommunications* **13**, pp. 106–110 (2006).

[23] Y. Choi, J. U. Won, and J. H. Park, "An experimental testbed for parcel handling with RFID technology", in *Proc. 8th International Conference on Advanced Communication Technology*, pp. 321–326 (2006).

[24] K. Coyle, "Management of RFID in libraries", *Journal of Academic Librarianship* **31**, pp. 486–489 (2005).

[25] M. S. Selamat and B. Y. Majlis, "Challenges in implementing RFID tag in a conventional library", in *Proc. 2006 IEEE International Conference on Semiconductor Electronics*, pp. 258 – 262 (2006).

[26] D. E. N. Davis, M. J. Withers, and R. P. Claydon, "Passive coded transponder using an acoustic-surface-wave delay line", *Electron. Lett.* **11**, pp. 163–164 (1975).

[27] J. Curie and P. Curie, "Développement, par pression, de l'électricité polaire dans les cristaux hémièdres à face inclinées", *Comptes rendus hebdomadaires des séances de l'Académie des sciences* **91**, pp. 294–295 (1880).

[28] J. Curie and P. Curie, "Contractions et dilatations produites par des tensions électriques dans les cristaux hémièdres à face inclinées", *Comptes rendus hebdomadaires des séances de l'Académie des sciences* **93**, pp. 1137–1140 (1881).

[29] R. M. White and F. W. Voltmer, "Direct piezoelectric coupling to surface elastic waves", *Appl. Phys. Lett.* **7**, pp. 314–316 (1965).

[30] P. H. Cole and R. Vaughan, "Electronic surveillance system", 1972, U. S. Patent no. 3706094.

[31] C. S. Hartmann, "Future high volume applications of SAW devices", in *Proc. 1985 IEEE Ultrasonics Symposium*, pp. 64–73 (1985).

[32] M. Epstein, "Passive transponders using acoustic surface wave devices", 1977, U. S. Patent no. 4059831.

[33] H. Skeie, "Surface acoustic wave passive transponder having parallel acoustic wave paths", 1986, U. S. Patent no. 4620191.

[34] V. P. Plessky, S. N. Kondratiev, R. Stierlin, and F. Nyffeler, "SAW tags: new ideas", in *Proc. 1995 IEEE Ultrasonics Symposium*, pp. 117–120 (1995).

[35] W. R. Holland, "Electronic surveillance and identification", 1988, U. S. Patent no. 4746830.

[36] H. Skeie, "Surface acoustic wave passive transponder having acoustic wave reflectors", 1986, U. S. Patent no. 4625208.

[37] L. Reindl, T. Ostertag, and W. Ruile, "SAW identification or sensor configuration operating with surface acoustic waves", 2000, U. S. Patent no. 6121892.

[38] R. Stierlin and R. Küng, "Process for carrying out a non-contact remote enquiry", 2002, U. S. Patent no. 6407695.

[39] L. Reindl and I. M. Shrena, "Wireless measurement of temperature using surface acoustic waves sensors", *IEEE Trans. Ultrason. Ferroelectr. Freq. Control* **51**, pp. 1457–1463 (2004).

[40] H. Engan, "Interdigital electrode transducers for the excitation of elastic surface waves in piezoelectric media", 1967, Electronics Lab., Norwegian Institute of Technology, Trondheim, Norway, ELAB Rept. TE-91.

[41] J. H. Collins, H. M. Gerard, T. M. Reeder, and H. J. Shaw, "Unidirectional surface wave transducer", *Proc. IEEE* **57**, pp. 833–835 (1969).

[42] K. Yamanouchi, F. M. Nyffeler, and K. Shibayama, "Low insertion loss acoustic surface wave filter using group-type unidirectional interdigital transducer", in *Proc. 1975 IEEE Ultrasonics Symposium*, vol. 1, pp. 317-321 (1975).

[43] F. G. Marshall, E. G. S. Paige, and A. S. Young, "New unidirectional transducer and broadband reflector of acoustic surface waves", *Electron. Lett.* **7**, pp. 638–640 (1971).

[44] F. G. Marshall and E. G. S. Paige, "Novel surface-acoustic-wave directional coupler with diverse applications", *Electron. Lett.* **7**, pp. 460–462 (1971).

[45] F. G. Marshall and E. G. S. Paige, "Observed properties of an acoustic-surface-wave multistrip coupler", *Electron. Lett.* **7**, pp. 463–464 (1971).

[46] C. S. Hartmann, W. S. Jones, and H. Vollers, "Wideband unidirectional interdigital surface wave transducer", *IEEE Trans. Sonics Ultrason.* **19**, pp. 378–381 (1972).

[47] R. C. Rosenfeld, R. B. Brown, and C. S. Hartmann, "Unidirectional acoustic surface wave filters with 2 dB insertion loss", in *Proc. 1974 IEEE Ultrasonics Symposium*, pp. 425–428 (1974).

[48] C. S. Hartmann, P. V. Wright, R. J. Kansy, and E. M. Garber, "An analysis of SAW interdigital transducers with internal reflections and the application to the design of single-phase unidirectional transducers", in *Proc. 1982 IEEE Ultrasonics Symposium*, pp. 40–45 (1982).

[49] M. Lewis, "Low loss SAW devices employing single stage fabrication", in *Proc. 1983 IEEE Ultrasonics Symposium*, pp. 104–108 (1983).

[50] M. F. Lewis, "Group-type unidirectional SAW devices employing intra-transducer reflector banks", *Electron. Lett.* **19**, pp. 1085–1087 (1983).

[51] K. Yamanouchi and H. Furuyashiki, "New low-loss SAW filter using internal floating electrode reflection types of single-phase unidirectional transducer", *Electron. Lett.* **20**, pp. 989–990 (1984).

[52] M. Takeuchi and K. Yamanouchi, "Coupled mode analysis of SAW floating electrode type unidirectional transducers", *IEEE Trans. Ultrason. Ferroelectr. Freq. Control* **40**, pp. 648–658 (1993).

[53] T. Kodama, H. Kawabata, Y. Yasuhara, and H. Sato, "Design of low-loss SAW filters employing distributed acoustic reflection transducers", in *Proc. 1986 IEEE Ultrasonics Symposium*, vol. 1, pp. 59-64 (1986).

[54] C. S. Hartmann and B. P. Abbot, "Overview of design challenges for single phase unidirectional SAW filters", in *Proc. 1989 IEEE Ultrasonics Symposium*, pp. 79–89 (1989).

[55] P. V. Wright, "The natural single-phase unidirectional transducer: a new low-loss SAW transducer", in *Proc. 1985 IEEE Ultrasonics Symposium*, vol. 1, pp. 58-63 (1985).

[56] P. Ventura, M. Solal, P. Dufilié, J. M. Hodé, and F. Roux, "A new concept in SPUDT design: the RSPUDT (resonant SPUDT)", in *Proc. 1994 IEEE Ultrasonics Symposium*, vol. 1, pp. 1-6 (1994).

[57] P. V. Wright, D. F. Thompson, and R. E. Chang, "Single-phase unidirectional transducers employing uniform-width dithered electrodes", in *Proc. 1995 IEEE Ultrasonics Symposium*, vol. 1, pp. 27-32 (1995).

[58] C. Jian and S. Beaudin, "A new type SPUDT SAW for use in high frequency around 2 GHz", in *Proc. 2002 IEEE Ultrasonics Symposium*, vol. 1, pp. 279-282 (2002).

[59] S. Lehtonen, V. P. Plessky, C. S. Hartmann, and M. M. Salomaa, "Unidirectional SAW transducer for gigahertz frequencies", *IEEE Trans. Ultrason. Ferroelectr. Freq. Control* **50**, pp. 1404–1406 (2003).

[60] S. Lehtonen, V. P. Plessky, C. S. Hartmann, and M. M. Salomaa, "SPUDT filters for the 2.45 GHz ISM band", *IEEE Trans. Ultrason. Ferroelectr. Freq. Control* **51**, pp. 1697–1703 (2004).

[61] C. S. Hartmann and V. P. Plessky, "Single phase unidirectional surface acoustic wave transducer and improved reflectors", 2007, U. S. Patent no. 7173360.

[62] E. Dai and G. Feng, "Passive and remote sensing based upon surface acoustic wave in special environments", in *Proc. 1997 IEEE MTT-S International Microwave and Optoelectronics Conference*, vol. 1, pp. 133 - 139 (1997).

[63] C. Hartmann, P. Brown, and J. Bellamy, "Design of global SAW RFID tag devices", in *Proc. 2nd International Symposium on Acoustic Wave Devices for Future Mobile Communication Systems*, pp. 15–19 (2004).

[64] L. Reindl and W. Ruile, "Programmable reflectors for SAW-ID-tags", in *Proc. 1993 IEEE Ultrasonics Symposium*, vol. 1, pp. 125-130 (1993).

[65] M. Epstein and B. W. Jordan, "Identification system using coded passive transponders", 1978, U. S. Patent no. 4096477.

[66] S. D. Moore, "Programmable phase coded surface wave device", 1976, U. S. Patent no. 3961290.

[67] H. Skeie, "Surface acoustic wave passive transponder having amplitude and phase-modifying surface pads", 1986, U. S. Patent no. 4625207.

[68] X. Q. Bao, W. Burkhard, V. V. Varadan, and V. K. Varadan, "SAW temperature sensor and remote reading system", in *Proc. 1987 IEEE Ultrasonics Symposium*, pp. 583–585 (1987).

[69] C. Campbell, *Surface Acoustic Wave Devices and Their Signal Processing Applications*. San Diego, USA: Academic Press, Inc., 1989, see p. 20.

[70] C. S. Hartmann, "A global SAW ID tag with large data capacity", in *Proc. 2002 IEEE Ultrasonics Symposium*, vol. 1, pp. 65-69 (2002).

[71] C. S. Hartmann, "Surface acoustic wave identification tag having enhanced data content and methods of operation and manufacture thereof", 2005, U. S. Patent no. 6966493.

[72] D. Porcino and W. Hirt, "Ultra-wideband radio technology: potential and challenges ahead", *IEEE Communications Magazine* **41**, pp. 66–74 (2003).

[73] Federal Communications Commission, "Revision of part 15 of the Commissions rules regarding ultra-wideband transmission systems", 2002, First Report and Order, ET Docket 98-153, FCC 02-48.

[74] G. Breed, "A summary of FCC rules for ultra wideband communications", *High Frequency Electronics* **4**, pp. 42–44 (2005).

[75] Federal Communications Commission, "Technical requirements applicable to all UWB devices", Code of Federal Regulations, Title 47, Chapter I, Part 15, §15.521.

[76] The Commission of the European Communities, "Commission decision of 21 February 2007 on allowing the use of the radio spectrum for equipment using ultra-wideband technology in a harmonised manner in the Community", *Official Journal of the European Union* **50**, pp. 33–36 (2007).

[77] Office of Communications, "Decision to make the wireless telegraphy (ultra-wideband equipment) (exemption) regulations 2007", 2007, Statement.

[78] A. Pohl, G. Ostermayer, L. Reindl, and F. Seifert, "Spread spectrum techniques for wirelessly interrogable passive SAW sensors", in *Proc. IEEE 4th International Symposium on Spread Spectrum Techniques and Applications*, vol. 2, pp. 730-734 (1996).

[79] F. Schmidt, O. Sczesny, C. Ruppel, and V. Mágori, "Wireless interrogator system for SAW-identification-marks and SAW-sensor components", in *Proc. 1996 IEEE International Frequency Control Symposium*, pp. 208–215 (1996).

[80] A. Springer, M. Huemer, L. Reindl, C. Ruppel, A. Pohl, F. Seifert, W. Gugler, and R. Weigel, "A robust ultra-broad-band wireless communication system using SAW chirped delay lines", *IEEE Trans. Microwave Theory Tech.* **46**, pp. 2213–2219 (1998).

[81] A. Pohl, M. Brandl, R. Steindl, L. Reindl, and F. Seifert, "Gated chirps for signal processing and communication engineering", in *Proc. 1998 IEEE Ultrasonics Symposium*, vol. 1, pp. 359-362 (1998).

[82] M. Chomiki, "SAW-based solutions for UWB communications", in *2005 European Microwave Conference*, vol. 3 (2005).

[83] Nanotron Technologies, "nanoNET chirp based wireless networks", http://www.nanotron.com.

[84] S. Li, L. Ma, and D. Wang, "A remote wireless identification system based on passive surface acoustic wave (SAW) devices", in *Proc. 2005 International Conference on Communications, Circuits and Systems*, vol. 2, pp. 1113-1116 (2005).

[85] T. Sugiura, T. Sato, E. Otobe, K. Tanji, N. Otani, H. Nagasaka, M. Hasegawa, and T. Shimamori, "Ultra-low power UWB communication system using SAW matched filters", in *Proc. 2005 IEEE Ultrasonics Symposium*, pp. 810–814 (2005).

[86] R. Brocato, J. Skinner, G. Wouters, J. Wendt, E. Heller, and J. Blaich, "Ultra-wideband SAW correlator", *IEEE Trans. Ultrason. Ferroelectr. Freq. Control* **53**, pp. 1554–1556 (2006).

[87] D. Puccio, D. Malocha, N. Saldanha, D. Gallagher, and J. Hines, "Orthogonal frequency coding for SAW tagging and sensors", *IEEE Trans. Ultrason. Ferroelectr. Freq. Control* **53**, pp. 377–384 (2006).

[88] D. Gallagher, D. Malocha, D. Puccio, and N. Saldanha, "Orthogonal frequency coded filters for use in ultra-wideband communication systems", *IEEE Trans. Ultrason. Ferroelectr. Freq. Control* **55**, pp. 696–703 (2008).

[89] E. Mariani, "Passive SAW-ID tags using a chirp transducer", 1995, U. S. Patent no. 5469170.

[90] T. Yoshihiko, "SAW-ID-tag device using chirp signal", 1999, Patent no. JP11145874.

[91] Z. Ianelli and M. Koslar, "Surface-wave transducer device and identification system with such device", 2004, U. S. Patent no. 6788204.

[92] W. J. Skudera, "Recognition tag for use in a system for identifying distant items", 1998, U. S. Patent no. 5734326.

[93] A. Stelzer, M. Pichler, S. Scheiblhofer, and S. Schuster, "Identification of SAW ID-tags using an FSCW interrogation unit and model-based evaluation", *IEEE Trans. Ultrason. Ferroelectr. Freq. Control* **51**, pp. 1412–1420 (2004).

[94] D. C. Malocha, J. Pavlina, D. Gallagher, N. Kozlovski, B. Fisher, N. Saldanha, and D. Puccio, "Orthogonal frequency coded SAW sensors and RFID design principles", in *Proc. 2008 IEEE Frequency Control Symposium*, pp. 278–283 (2008).

[95] C. E. Shannon, "A mathematical theory of communication", *The Bell System Technical Journal* **27**, pp. 379–423, 623–656 (1948).

[96] R. H. Tancrell, M. B. Schulz, H. H. Barrett, J. L. Davis, and M. G. Holland, "Dispersive delay lines using ultrasonic surface waves", *Proc. IEEE* **57**, pp. 1211–1213 (1969).

[97] R. C. Williamson and H. I. Smith, "Large-time-bandwidth-product surface-wave pulse compressor employing reflective gratings", *Electron. Lett.* **8**, pp. 401–402 (1972).

[98] R. C. Williamson and H. I. Smith, "The use of surface-elastic-wave reflection gratings in large time-bandwidth pulse-compression filters", *IEEE Trans. Sonics Ultrason.* **20**, pp. 113–123 (1973).

[99] R. C. Williamson and E. Stern, "Surface wave devices", 1975, U. S. Patent no. 3883831.

[100] L. P. Solie, "Reflective dot array for acoustic wave processing", 1977, U. S. Patent no. 4055820.

[101] H. van de Vaart and L. P. Solie, "A SAW pulse compression filter using the reflective dot array", in *MTT-S International Microwave Symposium Digest*, pp. 321–323 (1977).

[102] F. Huang, E. G. S. Paige, and D. R. Selviah, "High-performance SAW dispersive delay line using reflective thin metal dots", *Electron. Lett.* **22**, pp. 653–654 (1986).

[103] F. G. Marshall, E. G. S. Paige, and A. S. Young, "Amplitude weighting of SAW reflecting array-structures", in *Proc. 1974 IEEE Ultrasonics Symposium*, pp. 202–204 (1974).

[104] R. D. Weglein and O. W. Otto, "Characteristics of periodic acoustic-surface-wave grating filters", *Electron. Lett.* **10**, pp. 68–69 (1974).

[105] J. T. Godfrey, C. E. Nothnick, J. Schellenberg, R. A. Moore, and C. H. Grauling, "Phase-weighted metallized reflective arrays", in *Proc. 1976 IEEE Ultrasonics Symposium*, pp. 406–410 (1976).

[106] R. E. Chapman, R. K. Chapman, D. P. Morgan, and E. G. S. Paige, "In-line reflective array devices", in *Proc. 1978 IEEE Ultrasonics Symposium*, pp. 728–733 (1978).

[107] R. C. Woods, "Dispersive delay lines using 180° reflecting metal dot arrays", in *Proc. 1982 IEEE Ultrasonics Symposium*, pp. 88–91 (1982).

[108] F. Huang, "Correction factor for low-loss 180° reflecting linear chirp arrays in SAW devices", *IEEE Trans. Ultrason. Ferroelectr. Freq. Control* **35**, pp. 61–65 (1988).

[109] B. R. Potter and C. S. Hartmann, "Surface acoustic wave slanted device technology", *IEEE Trans. Sonics Ultrason.* **26**, pp. 411–418 (1979).

[110] S. M. Balashov, V. P. Plessky, C.-U. Kim, C.-W. Nam, and V. I. Grigorievsky, "Dispersive delay lines based on the use of narrow open metal reflectors and fan transducer", in *Proc. 2005 IEEE Ultrasonics Symposium*, pp. 2166–2169 (2005).

[111] J. Gong, Y. Zhang, X. Zhou, and P. Hartogh, "Wide bandwidth SAW chirp filters with improved magnitude response", in *Proc. 2006 IEEE Ultrasonics Symposium*, pp. 1895–1898 (2006).

[112] E. L. Cambiaggio and F. C. Cuozzo, "SAW reflection from conducting strips on LiNbO$_3$", *IEEE Trans. Sonics Ultrason.* **26**, pp. 340–344 (1979).

[113] E. G. S. Paige, A. G. Stove, and R. C. Woods, "SAW reflection from aluminium strips on LiNbO$_3$", in *Proc. 1981 IEEE Ultrasonics Symposium*, pp. 144–147 (1981).

[114] P. V. Wright, "Modeling and experimental measurements of the reflection properties of SAW metallic gratings", in *Proc. 1984 IEEE Ultrasonics Symposium*, pp. 54–63 (1984).

[115] D. Chen and H. A. Haus, "Analysis of metal-strip SAW gratings and transducers", *IEEE Trans. Sonics Ultrason.* **32**, pp. 395–408 (1985).

[116] K. Yamanouchi, G. Shimizu, and K. Morishita, "2.5 GHz-range SAW propagation and reflection characteristics and application to passive electronic tag and matched filter", in *Proc. 1993 IEEE Ultrasonics Symposium*, vol. 2, pp. 1267-1270 (1993).

[117] J. C. Crabb, J. D. Maines, and N. R. Ogg, "Surface-wave diffraction on LiNbO$_3$", *Electron. Lett.* **7**, pp. 253–255 (1971).

[118] S. Lehtonen, V. P. Plessky, C. S. Hartmann, and M. M. Salomaa, "Short reflectors operating at the fundamental and second harmonics on 128º LiNbO$_3$", *IEEE Trans. Ultrason. Ferroelectr. Freq. Control* **51**, pp. 343–351 (2004).

[119] S. Lehtonen, V. P. Plessky, N. Bereux, and M. M. Salomaa, "Minimum-loss short reflectors on 128º LiNbO$_3$", *IEEE Trans. Ultrason. Ferroelectr. Freq. Control* **51**, pp. 1203–1205 (2004).

[120] S. Lehtonen, V. P. Plessky, N. Bereux, and M. M. Salomaa, "Phases of the SAW reflection and transmission coefficients for short reflectors on 128º LiNbO$_3$", *IEEE Trans. Ultrason. Ferroelectr. Freq. Control* **51**, pp. 1671–1682 (2004).

[121] W. Wang, T. Han, X. Zhang, H. Wu, and Y. Shui, "Rayleigh wave reflection and scattering calculation by source regeneration method", *IEEE Trans. Ultrason. Ferroelectr. Freq. Control* **54**, pp. 1445–1453 (2007).

[122] P. Ventura, J. M. Hodé, and B. Lopes, "Rigorous analysis of finite SAW devices with arbitrary electrode geometries", in *Proc. 1995 IEEE Ultrasonics Symposium*, vol. 1, pp. 257-262 (1995).

[123] P. Ventura, J. M. Hodé, M. Solal, J. Desbois, and J. Ribbe, "Numerical methods for SAW propagation characterization", in *Proc. 1998 IEEE Ultrasonics Symposium*, vol. 1, pp. 175-186 (1998).

[124] H. P. Reichinger and A. R. Baghai-Wadji, "Dynamic 2D analysis of SAW-devices including massloading", in *Proc. 1992 IEEE Ultrasonics Symposium*, vol. 1, pp. 7-10 (1992).

[125] G. Kovacs, M. Anhorn, H. E. Engan, G. Visintini, and C. C. W. Ruppel, "Improved material constants for LiNbO$_3$ and LiTaO$_3$", in *Proc. 1990 IEEE Ultrasonics Symposium*, pp. 435–438 (1990).

[126] D. Pozar, *Microwave Engineering.* New York, USA: John Wiley & Sons, Inc., 1998, see pp. 196-213.

[127] C. S. Hartmann and B. P. Abbot, "Experimentally determining the transduction magnitude and phase and the reflection magnitude and phase of SAW SPUDT structures", in *Proc. 1990 IEEE Ultrasonics Symposium*, vol. 1, pp. 37-42 (1990).

[128] J. W. Cooley and J. W. Tukey, "An algorithm for the machine calculation of complex Fourier series", *Mathematics of Computation* **19**, pp. 297–301 (1965).

[129] J. R. Pierce, "Coupling of modes of propagation", *J. Appl. Phys.* **25**, pp. 179–183 (1954).

[130] Y. Koyamada and S. Yoshikawa, "Coupled mode analysis of a long IDT", *Review of the Electrical Communication Laboratories* **27**, pp. 432–444 (1979).

[131] S. Lehtonen, V. P. Plessky, and M. M. Salomaa, "Extraction of the SAW attenuation parameter in periodic reflecting gratings", *IEEE Trans. Ultrason. Ferroelectr. Freq. Control* **52**, pp. 111–119 (2005).

[132] L. Rayleigh, "On waves propagating along the plane surface of an elastic solid", *Proc. London Math. Soc.* **17**, pp. 4–11 (1885).

[133] K. Shibayama, K. Yamanouchi, H. Sato, and T. Meguro, "Optimum cut for rotated Y-cut $LiNbO_3$ crystal used as the substrate of acoustic-surface-wave filters", *Proc. IEEE* **64**, pp. 595–598 (1976).

[134] T. Han, W. Wang, H. Wu, and Y. Shui, "Reflection and scattering characteristics of reflectors in SAW tags", *IEEE Trans. Ultrason. Ferroelectr. Freq. Control* **55**, pp. 1387–1390 (2008).

[135] K. Hashimoto, *Surface Acoustic Wave Devices in Telecommunications.* Berlin, Germany: Springer, 2000, see p. 8.

[136] T. Kodama, "Broad-band compensation for diffraction in surface acoustic wave filters", *IEEE Trans. Sonics Ultrason.* **30**, pp. 127–136 (1983).

[137] J. Machui and W. Ruile, "Z-path IF-filters for mobile telephones", in *Proc. 1992 IEEE Ultrasonics Symposium*, vol. 1, pp. 147-150 (1992).

[138] F. G. Marshall and E. G. S. Paige, "Mode conversion in surface-acoustic-wave reflective arrays", *Electron. Lett.* **10**, pp. 137–138 (1974).

[139] J. Koskela, private communication, 2006.

[140] D. Royer and E. Dieulesaint, *Elastic Waves in Solids I, Free and Guided Propagation*. Berlin, Germany: Springer, 2000, see p. 251.

[141] J. Kuypers, A. Randles, M. Schmidt, S. Tanaka, and M. Esashi, "MEMS-based SAW devices", in *Proc. 3rd International Symposium on Acoustic Wave Devices for Future Mobile Communication Systems*, pp. 57–68 (2007).

[142] D. Morgan, *Surface-Wave Devices for Signal Processing*. Amsterdam: Elsevier, 1991, see pp. 220-222.

[143] C. S. Hartmann, D. T. Bell, and R. C. Rosenfeld, "Impulse model design of acoustic surface-wave filters", *IEEE Trans. Sonics Ultrason.* **20**, pp. 80–93 (1973).

[144] J. H. Kuypers, L. M. Reindl, S. Tanaka, and M. Esashi, "Maximum accuracy evaluation scheme for wireless SAW delay-line sensors", *IEEE Trans. Ultrason. Ferroelectr. Freq. Control* **55**, pp. 1640–1652 (2008).

Abstracts of Publications

I Narrow, open-circuited aluminum electrodes can provide controllable, weak reflectivity necessary for many applications such as surface acoustic wave (SAW) tags and dispersive delay lines (DDLs). We show, using finite- and boundary element method (FEM-BEM) based simulations and experiments, that a reflectivity of 0.3% per wavelength can be achieved easily and controlled by varying the electrode width.

II Reflectors comprised of only a single or a few electrodes provide controllable, weak reflectivity essential for surface acoustic wave (SAW) radio-frequency identification (RFID) tags. The reflection, transmission, and scattering parameters of such reflectors must be known as a function of frequency in order to be able to control the amplitudes of tag responses and to use phase-based encoding reliably.

In this work, we present a method of extracting the main reflection, transmission, and scattering parameters for short metal reflectors as a function of frequency. We use test device S parameters obtained through finite- and boundary-element method (FEM-BEM) based simulations and, as an example, determine the reflection and transmission coefficients (their absolute values and phase angles) and the energy scattered into bulk for a few different single-electrode reflectors. We compare these parameter values to earlier results.

Although only used for simulated data in this work, the same method can be applied to measured data as well. Assuming the S parameters available, this method is very fast and does not require any heavy calculation or special software.

III Surface acoustic wave (SAW) radio-frequency identification (RFID) tags are soon expected to be produced in very high volumes. The size and cost of a SAW RFID tag will be key parameters for many applications. Therefore, it is of primary importance to reduce the chip size. In this work, we describe the design principles of a 2.4-GHz SAW RFID tag that is significantly smaller than earlier reported tags. We also present simulated and experimental results.

The coded signal should arrive at the reader with a certain delay (typically about 1 μs), i.e., after the reception of environmental echoes. If the tag uses a bidirectional interdigital transducer (IDT), space for the initial delay is needed on both sides of the IDT. In this work, we replace the bidirectional IDT by a unidirectional one. This halves the space required by the initial delay because all the code reflectors must now be placed on the same side of the IDT. We reduce tag size even further by using a Z-path geometry in which the same space in
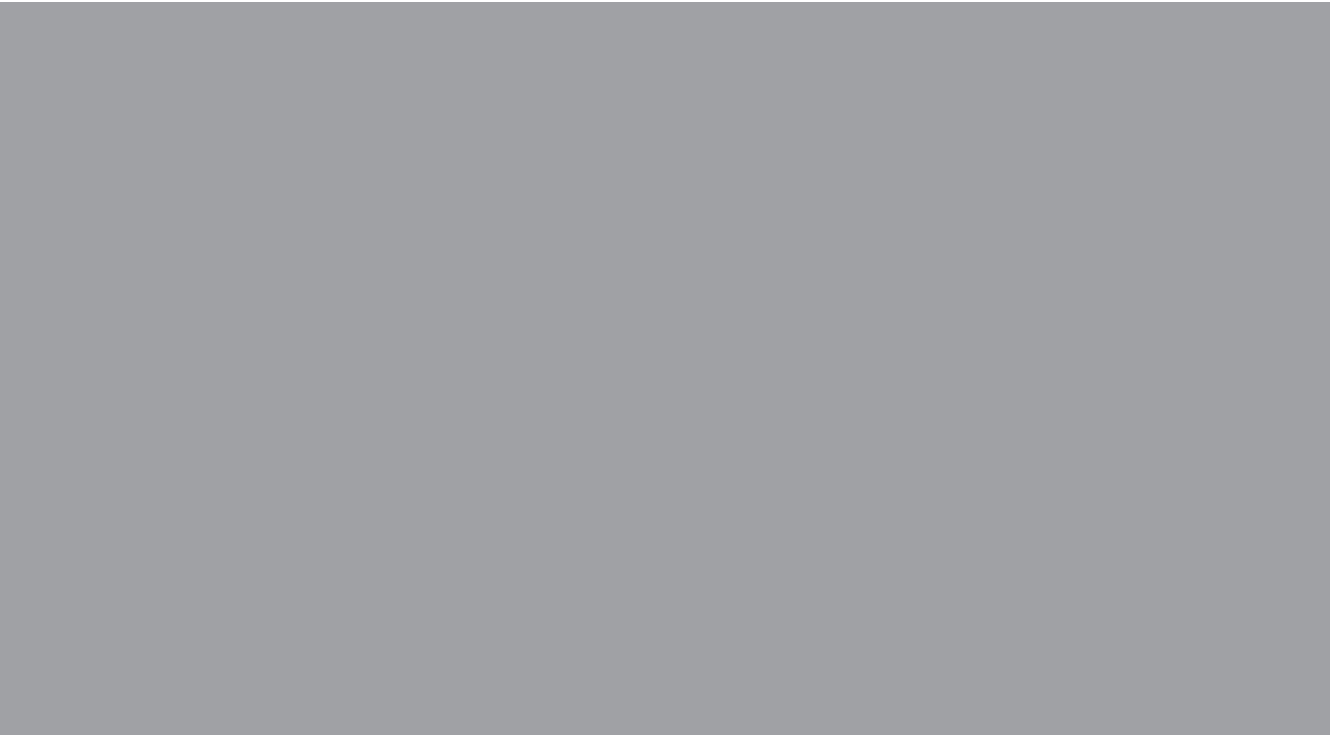
x-direction is used for both the initial delay and the code reflectors. Chip length is thus determined only by the space required by the code reflectors.

IV Surface acoustic wave (SAW) radio-frequency identification (RFID) tags are encoded according to partial reflections of an interrogation signal by short metal reflectors. The standard encryption method involves time position encoding that uses time delays of response signals. However, the data capacity of a SAW RFID tag can be significantly enhanced by extracting additional phase information from the tag responses.

In this work, we have designed, using FEM-BEM simulations, and fabricated, on $128°$-LiNbO$_3$, inline 2.44-GHz SAW RFID tag samples that combine time position and phase encoding. Each reflective echo has 4 possible time positions and a phase of $0°$, $-90°$, $-180°$, or $-270°$. This corresponds to 16 different states, i.e., 4 bits of data, per code reflector. In addition to the enhanced data capacity, our samples also exhibit a low loss level of -38 dB for code reflections.

V We discuss the feasibility of surface acoustic wave (SAW) radio-frequency identification (RFID) tags that rely on ultra-wideband (UWB) technology. We propose a design of a UWB SAW tag, carry out numerical experiments on the device performance, and study signal processing in the system. We also present experimental results for the proposed device and estimate the potentially achievable reading distance.

UWB SAW tags will have an extremely small chip size (< 0.5 x 1 mm^2) and a low cost. They also can provide a large number of different codes. The estimated read range for UWB SAW tags is about 2 m with a reader radiating as low as < 0.1-mW power levels with an extremely low duty factor.